Axion term in topological insulators with broken time reversal and parity

by

Itamar Reis

B.Sc, University of Tel-Aviv, 2010

A THESIS SUBMITTED IN PARTIAL FULFILLMENT
OF THE REQUIREMENTS FOR THE DEGREE OF

Master of Science

in

THE FACULTY OF GRADUATE AND POSTDOCTORAL
STUDIES
(Physics)

The University Of British Columbia
(Vancouver)

March 2014

Abstract

The main subject of this work is the axion term in the effective electromagnetic action of topological insulators, which is responsible for the special electromagnetic properties of these materials. The axion term is characterized by a parameter θ, which can only take the values of 0, for regular insulators, or π, for topological insulators, respecting at least one of the time reversal or parity symmetries. A non zero axion term leads to a variety of measurable phenomena, generally referred to as the magneto-electric effects.

We focus our interest on the value the parameter θ takes for a topological insulator, when both time reversal and parity are broken. In this case θ no longer must be quantized to 0 or π. We use a lattice model for a topological insulator, and introduce a symmetry breaking term in the Hamiltonian. We numerically find the value of θ in this case using calculations of the magnitude of various magneto-electric effects. The results are compared to the theoretical prediction. We find that θ is no longer quantized when a specific symmetry breaking term is introduced.

Preface

This dissertation is unpublished work, ultimately based on results from a numerical calculation. These results are compared with known theoretical predictions. The code for the calculation was written by the author, I. Reis. The diagrammatic theoretical calculation found in chapter 2 was carried out by my supervisor M. Franz.

Table of Contents

List of Figures

Acknowledgments

I would like to thank my supervisor M. Franz for introducing me to the subject and for his advice and comments throughout the work on this thesis. Thanks also goes to D. Marchand for his help with computational issues and to M. Vazifeh for suggestions during the weekly group meetings.

Dedication

Dedicated to B., Z., B. and S.

Chapter 1

Introduction

A special property of topological insulators is a unique effective electromagnetic action (ref. [1] and [2]). Like all insulators, the effective electromagnetic action inside topological insulators contains the regular part

$$S_0 = \frac{1}{2}\int d^4x \left(\epsilon\mathbf{E}^2 - \frac{1}{\mu}\mathbf{B}^2\right), \tag{1.1}$$

but unlike regular insulators, for topological insulators there is an extra term, called the axion term. That is, for topological insulators the effective electromagnetic action is $S = S_0 + S_\theta$, with

$$S_\theta = \int d^4x \frac{\theta}{2\pi}\frac{e^2}{2\pi}\mathbf{E}\cdot\mathbf{B} = \int d^4x \frac{\theta\alpha}{\pi}\mathbf{E}\cdot\mathbf{B}. \tag{1.2}$$

Here α, the fine structure constant, is

$$\alpha = \frac{e^2}{4\pi}. \tag{1.3}$$

We work in natural units

$$\hbar = c = 1. \tag{1.4}$$

The two Maxwell's equations that are altered due to the axion term are Gauss' and Ampere's laws

$$\begin{aligned} \nabla \cdot \mathbf{E} &= \rho - \frac{e^2}{4\pi^2} \nabla\theta \cdot \mathbf{B} \\ \nabla \times \mathbf{B} &= \frac{\partial \mathbf{E}}{\partial t} + \mathbf{j} + \frac{e^2}{4\pi^2} \left(\nabla\theta \times \mathbf{E} + \frac{\partial \theta}{\partial t} \mathbf{B} \right). \end{aligned} \tag{1.5}$$

The name 'axion' comes from the name of a hypothetical elementary particle, suggested in ref. [3] in 1977 and later discussed in ref [4] and [5], in relation to the problem of strong charge parity, in the field of Quantum chromodynamics. The effect of such a particle on electromagnetism in vacuum was found in 1987 by F. Wilczek (ref. [6]). In his paper he shows that the existence of the axion particle will create an additional term in the effective electromagnetic action, equal to the above axion term.

In the years past since their prediction, axions were not experimentally discovered. Searches still continue today, the axion being a possible dark matter composite (ref [7], [8] and [9]). Although the axion itself was not found yet, its effective electromagnetic action, the axion term, does appear in nature, in topological insulators. The difference between the two cases is the physical interpretation of θ. For axions it is the field of the particle, and for topological insulators θ is a parameter describing the material.

At first look, the axion term might seem to break both time reversal and parity symmetries. We know that under parity: $\mathbf{E} \to -\mathbf{E}$ and $\mathbf{B} \to \mathbf{B}$, and so $S_\theta \to -S_\theta$. Under time reversal we have a similar story: $\mathbf{E} \to \mathbf{E}$ and $\mathbf{B} \to -\mathbf{B}$, and again $S_\theta \to -S_\theta$. What saves the day is the fact that the axion term is invariant to changes of 2π in the θ parameter. That is, the partition function and all physical quantities are not effected by the transformation $\theta \to \theta + 2\pi n$, where n is an integer. This is shown in ref. [10]. This fact tells us that $\theta = \pi$ is equivalent to $\theta = -\pi$, which means that with this value of θ, the axion term respects both $\mathcal{P}$ and $\mathcal{T}$. We see that we have exactly two options that respect the symmetries, $\theta = \pi$ and the trivial $\theta = 0$. For regular insulators of course $\theta = 0$, and for topological insulators we have $\theta = \pi$.

On a surface between topological insulators and regular insulators the value of θ needs to change from π to 0. Although $\mathcal{P}$ is generally broken on surfaces, $\mathcal{T}$ should still be respected. This fact does not allow θ to be changed continuously. The result is a conducting surface state for which θ is not defined, and as such allows the transition between 0 and π. The existence and the special properties of this surface state are the most interesting features of topological insulators.

The original theoretical proposal of topological insulators (ref. [11] and [12]) predict the existence of the metallic surface state. This surface state was also the smoking gun to be later experimentally discovered (ref. [13], [14] and [15]) in materials such as Bi_2Se_3 and Bi_2Te_3, to prove the existence of the topological insulator state of matter.

A different option for the surface between a topological insulator and a regular insulator appears when $\mathcal{T}$ is artificially broken on the surface, for example with a ferromagnetic film. In this case θ can change continuously and we can get the properties of the surface state from the axion term. The quantity of interest is the electric current on the surface

$$j^{\mu} = \frac{\partial \mathcal{L}}{\partial A_{\mu}}. \tag{1.6}$$

To get the current we write the axion term in a different form:

$$S_{\theta} = \int d^4x \mathcal{L}_{\theta} = \int d^4x \frac{\theta}{2\pi} \frac{e^2}{16\pi} \epsilon_{\mu\nu\alpha\beta} F^{\mu\nu} F^{\alpha\beta}. \tag{1.7}$$

The current is

$$j^{\mu} = \frac{e^2}{4\pi^2} \epsilon^{\mu\nu\alpha\beta} \partial_{\nu}\theta \partial_{\alpha} A_{\beta}. \tag{1.8}$$

From this current we can get the characteristics of the surface. For example a half quantized hall conductance, taking the z axis to be perpendicular to the surface we have

$$\begin{aligned} j_x &= \frac{1}{2}\frac{e^2}{h} E_y \rightarrow \\ \sigma_{xy} &= \frac{1}{2}\frac{e^2}{h}. \end{aligned} \tag{1.9}$$

Where this is the total current flowing in the region in which $\theta(z)$ changes from π to 0.

We saw that one can distinguish topological insulators from regular insulators by the value of θ. A different way to characterize insulators is with a Z_2 topological invariant as introduced in a series of papers by Fu, Kane and Mele (ref. [11], [12] and [16]). The motivation behind the definition of this topological invariant, called ν_0, is coming from the metallic surface states, as opposed to the definition of θ coming from the electromagnetic response. The definition is such that a material with non-zero ν_0 will have metallic surface states. Although defined very differently, there is an equivalence between θ and ν_0, as proved in ref. [17],

$$(-1)^{\nu_0} = e^{i\theta}. \tag{1.10}$$

Later we present the ways to calculate the topological invariants and do the calculation for a lattice model.

Next we turn to the case of a system with broken $\mathcal{T}$ and $\mathcal{P}$ symmetries. In this case the argument described above, for the quantization of the θ parameter, does not apply. In rest of the work we discuss the value θ takes for a topological insulator with broken symmetries.

Some discussions of this problem are found in the literature. Ref. [18] suggested the idea of a dynamical θ field. To have a dynamical θ field the first thing to do is remove the quantization condition from θ, this is done by breaking $\mathcal{T}$ and $\mathcal{P}$. In the paper a calculation of θ using band structure methods suggested that there is a correction to θ coming from a specific kind of symmetry breaking term. In this case the form of the correction is not discussed.

An explicit formula for the relation between θ and the magnitude of the symmetry breaking term can be found in ref. [19]. As will be discussed shortly, many properties of topological insulators can be described using field theory approach. In the paper this field theory description of topological insulators is used to find the form θ takes when the symmetries are broken. The same relation is obtained using a calculation similar to the one found in the well known paper by Goldstone and Wilczek in ref. [20].

In the next section we present the field theory calculation for θ. In later sections we test this prediction using a lattice model for a topological insulator, with a symmetry breaking term. We numerically find the value of θ in this case using calculations of the magnitude of magneto-electric effects, such as the Witten effect (ref. [21] and [22]) and charge accumulated in the flux insertion setup (ref. [23]). The results are also compared to a band structure calculation of θ, using the same lattice model. For the band structure calculation we follow formulas from ref. [1] and [18].

Chapter 2

Axion term in a system with broken symmetries

The electrons occupying the low energy states in a topological insulator behave as Dirac fermions and can be described by the Dirac Lagrangian

$$\mathcal{L} = \bar{\Psi}\gamma^{\mu}\left(i\partial_{\mu} - eA_{\mu}\right)\Psi + m\bar{\Psi}\Psi. \tag{2.1}$$

Many properties of topological insulators can be derived by only considering this low energy theory (ref. [1]). This fact is unique when compared to the much more complicated theories usually needed to understand material properties.

The appearance of the axion term in the effective electromagnetic action is one of the properties we can understand starting from the Lagrangian above. Starting from this Lagrangian we do a chiral rotation,

$$\Psi \to \exp\left(i\frac{\beta}{2}\gamma_5\right)\Psi, \tag{2.2}$$

where

$$\gamma_5 = i\gamma_0\gamma_1\gamma_2\gamma_3,\ \{\gamma_{\mu}, \gamma_5\} = 0,\ \gamma_5^2 = 1. \tag{2.3}$$

Due to the following property

$$\begin{aligned}\bar{\Psi} = \Psi^\dagger\gamma_0 \to \Psi^\dagger \exp\left(-i\frac{\beta}{2}\gamma_5\right)\gamma_0 \\ = \Psi^\dagger\gamma_0 \exp\left(i\frac{\beta}{2}\gamma_5\right) \\ = \bar{\Psi}\exp\left(i\frac{\beta}{2}\gamma_5\right),\end{aligned} \tag{2.4}$$

the only term in the Lagrangian effected by this transformation is the mass term

$$\begin{aligned}m\bar{\Psi}\Psi \to m\bar{\Psi}\exp\left(i\frac{\beta}{2}\gamma_5\right)\Psi \\ = m\cos\beta\bar{\Psi}\Psi + im\sin\beta\bar{\Psi}\gamma_5\Psi.\end{aligned} \tag{2.5}$$

The γ_5 term breaks both $\mathcal{P}$ and $\mathcal{T}$. The other effect of the transformation is coming from the path integral measure, using Fujikawa's method in ref. [24] we have

$$D\bar{\Psi}D\Psi \to D\bar{\Psi}D\Psi \exp\left(\int d^4x \frac{\beta}{2\pi}\frac{e^2}{16\pi}\epsilon_{\mu\nu\alpha\beta}F^{\mu\nu}F^{\alpha\beta}\right), \tag{2.6}$$

that is, this transformation creates an axion term in effective electromagnetic action. The θ parameter is changed by $\theta \to \theta + \beta$. If $\beta = \pi$ we get $m\bar{\Psi}\Psi \to -m\bar{\Psi}\Psi$,. We see that when the mass changes sign, θ changes between 0 and π. We note that θ is not determined for a specific sign of the mass. We can only say that it is changing between 0 and π (that is, from 0 to π, or from π to 0) when the sign of the mass changes. When $\beta \neq 0, \pi$ we get a non zero $\mathcal{P}$ and $\mathcal{T}$ breaking term in the Dirac Lagrangian, which allows a $\mathcal{P}$ and $\mathcal{T}$ breaking axion term in the effective electromagnetic action.

Next we review a more simple way to get the same result, the correction to θ due to $\mathcal{P}$ and $\mathcal{T}$ breaking. We start again from the Dirac Lagrangian

$$\mathcal{L} = \bar{\Psi}\gamma^\mu\left(i\partial_\mu - eA_\mu\right)\Psi + m\bar{\Psi}\Psi + m_5\bar{\Psi}i\gamma_5\Psi. \tag{2.7}$$

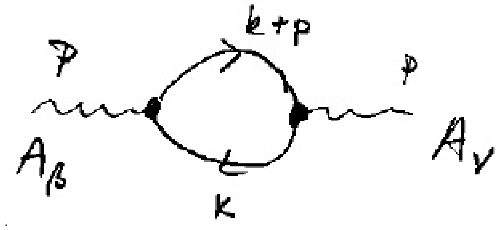

Figure 2.1: First Feynman diagram with fermionic contribution to the electromagnetic field propagator.

We want to check what would be the impact of adding a $\mathcal{P}$ and $\mathcal{T}$ breaking term on the value of θ. The formal way to do this is to integrate out the fermions. To do this one calculates the contribution to the electromagnetic field propagator, coming from the interaction with the fermions. The first Feynman diagram contributing to this is shown in Fig. 2.1. This diagram is UV-divergent with a result that depend on the regulator used.

Here we want to use a shortcut following ref. [20]. We use the electric current generated by the axion term, the 'axion current'

$$S_\theta = \int d^4x \mathcal{L}_\theta = \int d^4x \frac{\theta}{2\pi}\frac{e^2}{16\pi}\epsilon_{\mu\nu\alpha\beta}F^{\mu\nu}F^{\alpha\beta}$$

$$j^\mu = \frac{\partial \mathcal{L}}{\partial A_\mu} = \frac{e^2}{4\pi^2}\epsilon^{\mu\nu\alpha\beta}\partial_\nu\theta\partial_\alpha A_\beta.$$

We also evaluate the electric current starting from the electrons Lagrangian with a $\mathcal{P}$ and $\mathcal{T}$ breaking term, then match the result to the form of the axion current above. From this procedure we can see what is the relation between θ and the m_5. We evaluate

$$j^\mu = \frac{\partial \mathcal{L}}{\partial A_\mu} = e\bar{\Psi}\gamma^\mu\Psi, \tag{2.8}$$

in terms of the external fields $m_5(x)$ and $A_\mu(x)$. This is a perturbative calculation for the expectation value of the current $< \bar{\Psi}\gamma^\mu\Psi >$ using Feynman diagrams. m_5 is treated as a perturbation. The leading contribution

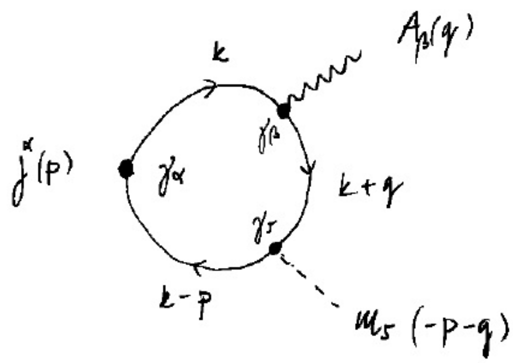

Figure 2.2: First Feynman diagram contributing to the electromagnetic current. This electromagnetic current is to be compared with the 'axion current', the 'axion current' being the current produced by a non-zero axion term in the effective electromagnetic action.

that gives an axion current form comes from the diagram shown in Fig. 2.2. There is also a diagram with m_5 and A_β interchanged giving the same contribution. This diagram gives

$$\begin{aligned}
< j^\alpha > &= e m_5(-p-q) A_\beta(q) \times \\
&\int \frac{d^4k}{(2\pi)^4} \mathrm{Tr}\left[\gamma^\alpha (\not k - m)^{-1} e \gamma^\beta (\not k + \not q - m)^{-1} \gamma_5 (\not k - \not p - m)^{-1}\right] \\
&= e^2 m_5(-p-q) A_\beta(q) \mathcal{Z}^{\alpha\beta}(p,q).
\end{aligned} \tag{2.9}$$

The fermion propagator is

$$\frac{1}{\not k - m} = \frac{\not k + m}{k^2 - m^2}, \tag{2.10}$$

and the slash notation is used

$$\not k = k^\mu \gamma_\mu. \tag{2.11}$$

We expand $\mathcal{Z}^{\alpha\beta}(p,q)$ to first order in p, q. As that is the order that appears in the axion current we expect to get

$$\mathcal{Z}^{\alpha\beta}(p,q) = p_\mu q_\nu \frac{\partial^2 \mathcal{Z}^{\alpha\beta}}{\partial p_\mu \partial q_\nu}\bigg|_{p,q=0}. \tag{2.12}$$

We use

$$\frac{\partial}{\partial p_\mu}(\not{k} - \not{p} - m)^{-1}\bigg|_{p=0} = -\frac{\gamma^\mu}{k^2 - m^2} + \frac{2k^\mu(\not{k} + m)}{(k^2 - m^2)^2}. \tag{2.13}$$

When the calculation is carried out all the contributions coming from the second term are found to add up to zero. We are left with only the first term

$$\mathcal{Z}^{\alpha\beta}(p,q) = p_\mu q_\nu \int \frac{d^4k}{(2\pi)^4}\frac{1}{(k^2 - m^2)^3}\mathrm{Tr}\left[\gamma^\alpha(\not{k} + m)\gamma^\beta\gamma^\nu\gamma_5(-1)\gamma^\mu\right]. \tag{2.14}$$

As a trace of an odd number of γ matrices is zero, we see that from the $(\not{k} + m)$ factor only the m contributes. We use

$$\mathrm{Tr}\left[\gamma^\alpha\gamma^\beta\gamma^\mu\gamma^\nu\gamma_5\right] = 4i\epsilon^{\alpha\beta\mu\nu}, \tag{2.15}$$

to get

$$\mathcal{Z}^{\alpha\beta}(p,q) = m p_\mu q_\nu 4i\epsilon^{\alpha\beta\mu\nu} \int \frac{d^4k}{(2\pi)^4}\frac{1}{(k^2 - m^2)^3} = m p_\mu q_\nu 4i\epsilon^{\alpha\beta\mu\nu} I(m^2). \tag{2.16}$$

The integral is carried out using analytic continuation to the complex plane $k \to i\mathcal{K}$,

$$I(m^2) = -i\frac{\Omega_4}{(2\pi)^4}\int_0^\infty d\mathcal{K}\frac{\mathcal{K}^3}{(\mathcal{K}^2 + m^2)^3} = \frac{-i}{32m^2\pi^2}, \tag{2.17}$$

where Ω_4 is the solid angle in 4 dimensions. We integrate over p and q to get the current in real space, we also add the factor of two coming from the second diagram

$$< j^\alpha >= \frac{e^2}{4\pi^2}\epsilon^{\alpha\beta\mu\nu}\frac{\partial_\mu m_5}{m}\partial_\nu A_\beta. \tag{2.18}$$

Remembering that we are working in the limit $m_5 \ll m$ and with a constant

m this result is equal to

$$< j^\alpha >= \frac{e^2}{4\pi^2}\epsilon^{\alpha\beta\mu\nu}\partial_\mu \arctan\left(\frac{m_5}{m}\right)\partial_\nu A_\beta. \tag{2.19}$$

When compared to the axion current coming from the axion term in the electromagnetic action, this leads to

$$\theta(m_5) = \arctan\left(\frac{m_5}{m}\right) + \text{Const.} \tag{2.20}$$

We know that when $m_5 = 0$, $\theta = 0, \pi$ and thus the constant is the above result can be 0 or π.

In ref. [19] the same result is obtained by a calculation of the electromagnetic field propagator. We note that it might look like there is a difference of a factor of two between the result above to the result from ref. [19]. This is resolved due to the fact that in ref. [19] the result is for the change in θ on a surface between a region with $+m, +m_5$ and a region with $-m, +m_5$. In this case if the correction to θ is indeed $\arctan\left(\frac{m_5}{m}\right)$, then on such a surface we would get a correction to the change in θ of $2\arctan\left(\frac{m_5}{m}\right)$.

Chapter 3

Numerical probing of the θ parameter in the axion term

We want to test the theoretical prediction numerically using a lattice model for a topological insulator. In order to numerically probe the value of θ one can make use of the magneto-electric effects generated by the axion term. All the effects we used can be derived from the axion current

$$j^{\mu} = \frac{e^2}{4\pi^2} \epsilon^{\mu\nu\alpha\beta} \partial_{\nu} \theta \partial_{\alpha} A_{\beta},$$

and specifically from the charge density

$$j^0 = \rho = \frac{e^2}{4\pi^2} \nabla\theta \cdot \mathbf{B}. \tag{3.1}$$

assuming θ does not depend on time, which is the case here. We numerically calculate this charge density in different setups and from the result deduce the value of θ.

3.1 Numerical model for a topological insulator

For the numerical calculation we use the method of exact diagonalization for a simple topological insulator model used in ref. [23] and [21]. First we introduce the model respecting time reversal and parity, later we add a symmetry breaking term. We take a cubic lattice with two orbitals per site, denoted c and d. The Hamiltonian consists of two parts, $H = H_{SO} + H_{cd}$. The first part is the spin orbit coupling

$$H_{SO} = i\lambda \sum_{j,\mu} \Psi_j^\dagger \tau_z \sigma_\mu \Psi_{j+\mu} + h.c. \tag{3.2}$$

Here $\Psi_j = (c_{j,\uparrow}, c_{j,\downarrow}, d_{j,\uparrow}, d_{j,\downarrow})^T$ where $c_j^\dagger, c_j$ are creation and annihilation operators for the c orbital in the j site. τ_i are the Pauli matrices in orbital space, σ_i are in spin space. $\mu = x, y, z$. The second part

$$H_{cd} = \epsilon \sum_j \Psi_j^\dagger \tau_x \Psi_j - t \sum_{j,\mu} \Psi_j^\mu \tau_x \Psi_{j+\mu} + h.c, \tag{3.3}$$

contains a spin dependent hopping term. In momentum space this Hamiltonian takes the form $H = \sum_{\mathbf{k}} \Psi_{\mathbf{k}}^\dagger \mathcal{H}_{\mathbf{k}} \Psi_{\mathbf{k}}$, where

$$\mathcal{H}_{\mathbf{k}} = -2\lambda \sum_\mu \tau_z \sigma_\mu \sin k_\mu + \tau_x m_{\mathbf{k}} \tag{3.4}$$

and

$$m_{\mathbf{k}} = \epsilon - 2t \sum_\mu \cos k_\mu. \tag{3.5}$$

This can be written as

$$\mathcal{H}_{\mathbf{k}} = \sum_{a=1}^{4} \Gamma_a d_a(\mathbf{k}), \tag{3.6}$$

with

$$\Gamma_a = (\tau_z \sigma_x, \tau_z \sigma_y, \tau_z \sigma_z, \tau_x) \tag{3.7}$$

and

$$d_a(\mathbf{k}) = (-2\lambda \sin k_x, -2\lambda \sin k_y, -2\lambda \sin k_z, m_{\mathbf{k}}). \tag{3.8}$$

3.1.1 The spectrum of the model

This Hamiltonian is easily diagonalized due to the fact that it is composed of anti commuting matrices. We can square the Hamiltonian to get $\mathcal{H}_{\mathbf{k}}^2 =$

$4\lambda^2 \sum_\mu \sin^2 k_\mu + m_{\mathbf{k}}^2$, and from this we get the spectrum

$$E_{\mathbf{k}} = \pm\sqrt{4\lambda^2 \sum_\mu \sin^2 k_\mu + m_{\mathbf{k}}^2}. \tag{3.9}$$

There are two bands, each band is doubly degenerate. This is due to the fact that there are four states per unit cell which gives four states per momentum $\mathbf{k}$. The gap between the bands can close at the following 8 points, called Γ points

$$\mathbf{\Gamma}_1 = (0,0,0) \tag{3.10}$$

$$\mathbf{\Gamma}_{2,3,4} = (\pi,0,0)\,,(0,\pi,0)\,,(0,0,\pi) \tag{3.11}$$

$$\mathbf{\Gamma}_{5,6,7} = (\pi,\pi,0)\,,(0,\pi,\pi)\,,(\pi,0,\pi) \tag{3.12}$$

$$\mathbf{\Gamma}_8 = (\pi,\pi,\pi)\,. \tag{3.13}$$

For $\mathbf{\Gamma}_1$ the gap will close for $\epsilon = 6t$, for $\mathbf{\Gamma}_{2,3,4}$ at $\epsilon = 2t$, for $\mathbf{\Gamma}_{5,6,7}$ at $\epsilon = -2t$ and for $\mathbf{\Gamma}_8$ at $\epsilon = -6t$.

The Γ points are also called time reversal invariant points, as at those points $\mathcal{H}_{\mathbf{k}}$ is invariant under time reversal (and also under parity). This is due to the fact that at those points $\mathbf{k} = -\mathbf{k}$, and as explained later $\mathcal{H}_{\mathbf{k}}$ transforms under time reversal to $\mathcal{H}_{-\mathbf{k}}$.

3.2 Topological phases

3.2.1 Using θ

One way to find the topological phases of this model is by using the band structure formula for θ (ref. [1])

$$\theta = \frac{1}{4\pi}\int_{BZ} d^3k \epsilon^{ijk}\ \mathrm{Tr}\left[A_i\partial_j A_k + i\frac{2}{3}A_iA_jA_k\right], \tag{3.14}$$

where $A_i^{\alpha\beta}$ is the Berry connection,

$$A_i^{\alpha\beta}(\mathbf{k}) = -i\left\langle \alpha\mathbf{k}\left|\frac{\partial}{\partial k_i}\right|\beta\mathbf{k}\right\rangle. \tag{3.15}$$

α, β are band labels, $|\alpha\mathbf{k}>$ are eigenfunctions of $\mathcal{H}_{\mathbf{k}}$. The trace is over occupied states. This formula for θ is generally hard to evaluate, but for the Dirac Hamiltonian in use here

$$\begin{aligned}
\mathcal{H}_{\mathbf{k}} &= \sum_{a=1}^{4}\Gamma_a d_a(\mathbf{k}) \\
\Gamma_a &= (\tau_z\sigma_x, \tau_z\sigma_y, \tau_z\sigma_z, \tau_x) \\
d_a(\mathbf{k}) &= (-2\lambda\sin k_x, -2\lambda\sin k_y, -2\lambda\sin k_z, m_{\mathbf{k}})
\end{aligned}$$

it is possible to get an analytical expression (ref. [21]). This is done by finding the eigenstates of the Hamiltonian. The expression is

$$\theta = \frac{1}{2\pi}\int_{BZ} d^3k\,\epsilon^{\alpha\beta\mu\nu}\frac{1}{|d(\mathbf{k})|^4} d_\alpha\partial_{k_x}d_\beta\partial_{k_y}d_\mu\partial_{k_z}d_\nu. \tag{3.16}$$

Following ref. [21], from the structure of the integral we see that in the limit of small mass, $m_{\mathbf{k}} \ll \lambda$, the contribution is coming only from the Γ points. In this limit for each Dirac point we expand $d_a(\mathbf{k})$ around $\mathbf{k} = \mathbf{\Gamma}$ to get

$$\theta_{\mathbf{\Gamma}} = \frac{1}{2\pi}\int d^3k\frac{v_{\mathbf{\Gamma},x}v_{\mathbf{\Gamma},y}v_{\mathbf{\Gamma},z}m_{\mathbf{\Gamma}}}{\left(4\lambda^2k^2 + m_{\mathbf{\Gamma}}^2\right)^2}, \tag{3.17}$$

where

$$v_{\mathbf{\Gamma},i} = -2\lambda\left(\cos\Gamma_x, \cos\Gamma_y, \cos\Gamma_z\right) \tag{3.18}$$

are the Dirac velocities. Due to the fact that the entire contribution is from small k we can take the integration limits to infinity and the integral gives

$$\theta_{\mathbf{\Gamma}} = -\frac{\pi}{2}\mathrm{sgn}\left(v_{\mathbf{\Gamma},x}v_{\mathbf{\Gamma},y}v_{\mathbf{\Gamma},z}m_{\mathbf{\Gamma}}\right). \tag{3.19}$$

The total θ is

$$\theta = \sum_{\mathbf{\Gamma}} \theta_{\mathbf{\Gamma}}. \tag{3.20}$$

This result is obtained in the limit of $m_{\mathbf{k}} \ll \lambda$, but it remains valid when the model parameters are continuously changed, as long as $m_{\mathbf{k}}$ does not go through zero at any of the Γ points. The reason is that θ can not change unless the gap closes, as θ is quantized to be either 0 or π for any insulator (with $\mathcal{P}$ or $\mathcal{T}$ symmetries). When the model parameters are changed continuously θ can not change unless a metallic state occurs, that is when the gap close.

The sign of the Dirac velocities only depends on λ, the sign of the masses depends on the relation between ϵ and t. We assume $\lambda, t > 0$. In this case we can write

$$\theta = \frac{\pi}{2} \left(-\text{sgn} \left(\epsilon + 6t \right) + 3\text{sgn} \left(\epsilon + 2t \right) - 3\text{sgn} \left(\epsilon - 2t \right) + \text{sgn} \left(\epsilon - 6t \right) \right). \tag{3.21}$$

The result for different values of ϵ is

	$\epsilon < -6t$	$-6t < \epsilon < -2t$	$-2t < \epsilon < 2t$	$2t < \epsilon < 6t$	$6t < \epsilon$
θ	0	π	0 (2π)	π	0

3.2.2 Using ν_0

A different but equivalent way of finding the topological phases of the model is by calculating the Z_2 invariant. For Hamiltonians with both $\mathcal{T}$ and $\mathcal{P}$ symmetries this can be done relatively easily, following ref. [12]. At the Γ points we have Kramer degenerate pairs of states which share the parity eigenvalue due to $[\mathcal{T}, \mathcal{P}] = 0$. The value of ν_0 is calculated from the parity eigenvalues at the Γ points. For every Γ point, we take the product of the parity eigenvalues over all the occupied bands, to get $\delta_{\mathbf{\Gamma}}$

$$\delta_{\mathbf{\Gamma}} = \prod_m \xi_m(\mathbf{\Gamma}), \tag{3.22}$$

where m is the index of the occupied Kramer pairs and $\xi_m = \pm 1$ is the parity eigenvalue of the pair. The Z_2 invariant is

$$(-1)^{\nu_0} = \prod_{\mathbf{\Gamma}} \delta_{\mathbf{\Gamma}}. \tag{3.23}$$

For the 4×4 Hamiltonian in use here we have, at half filling, one occupied Kramer pair for each Γ point. The Hamiltonian at the Γ points is

$$\mathcal{H}_{\mathbf{\Gamma}} = \tau_x m_{\mathbf{\Gamma}}, \tag{3.24}$$

and as explained in the next section, the parity operator (at the Γ points) is

$$\mathcal{P} = \tau_x. \tag{3.25}$$

In this case, for the negative energy states, the parity eigenvalue is $'+'$ if $m_{\mathbf{\Gamma}}$ is negative, and $'-'$ if $m_{\mathbf{\Gamma}}$ is positive, that is

$$\xi_{\mathbf{\Gamma}} = -\mathrm{sgn}(m_{\mathbf{\Gamma}}), \tag{3.26}$$

and

$$(-1)^{\nu_0} = \prod_{\mathbf{\Gamma}} \mathrm{sgn}(m_{\mathbf{\Gamma}}). \tag{3.27}$$

To get he final result we start from a small ϵ where all the $m_{\mathbf{\Gamma}}$s are negative and $\nu_0 = 0$. When we cross $\epsilon = -6t$, $m_{(\pi,\pi,\pi)}$ changes sign and we get $\nu_0 = 1$. We continue is this manner to get

	$\epsilon < -6t$	$-6t < \epsilon < -2t$	$-2t < \epsilon < 2t$	$2t < \epsilon < 6t$	$6t < \epsilon$
ν_0	0	1	0	1	0

3.3 $\mathcal{P}$ and $\mathcal{T}$ breaking term

In the numerical calculation we will want to break $\mathcal{T}$ and $\mathcal{P}$ in the bulk. To do this we need to know what operator form these symmetries take for the model in use here. Time Reversal for a single spin $\frac{1}{2}$ particle is implemented by $\mathcal{T} = \mathcal{K}\sigma_y$ where $\mathcal{K}$ is complex conjugate and σ_y is in spin space, $\mathcal{T}^2 = -1$.

$\mathcal{T}$ changes the direction of time and thus for momentum $\mathbf{k} \to -\mathbf{k}$ and for position $\mathbf{x} \to \mathbf{x}$.

We want to get a condition on the 4×4 $\mathcal{H}_k$ for the entire Hamiltonian $H = \sum_{\mathbf{k}} \Psi_{\mathbf{k}}^\dagger \mathcal{H}_{\mathbf{k}} \Psi_{\mathbf{k}}$ to be invariant under time reversal. We use the transformation rule for the creation and annihilation operators

$$\begin{aligned} \mathcal{T} c_j \mathcal{T}^{-1} &= c_j \\ \mathcal{T} c_{\mathbf{k}} \mathcal{T}^{-1} = \mathcal{T} \sum_j \exp{(ij\mathbf{k})} c_j \mathcal{T}^{-1} &= \sum_j \exp{(-ij\mathbf{k})} \mathcal{T} c_j \mathcal{T}^{-1} = c_{-\mathbf{k}}, \end{aligned} \tag{3.28}$$

where the minus sign in the exponent is due to the complex conjugate property. The transformation of the entire Hamiltonian is

$$\begin{aligned} \mathcal{T} \left(\sum_{\mathbf{k}} \Psi_{\mathbf{k}}^\dagger \mathcal{H}_{\mathbf{k}} \Psi_{\mathbf{k}} \right) \mathcal{T}^{-1} = \sum_{\mathbf{k}} \Psi_{-\mathbf{k}}^\dagger \mathcal{T} \mathcal{H}_{\mathbf{k}} \mathcal{T}^{-1} \Psi_{-\mathbf{k}} &= \sum_{\mathbf{k}} \Psi_{-\mathbf{k}}^\dagger \sigma_y \mathcal{H}_{\mathbf{k}}^\star \sigma_y \Psi_{-\mathbf{k}} \\ &= \sum_{\mathbf{k}} \Psi_{\mathbf{k}}^\dagger \mathcal{H}_{\mathbf{k}} \Psi_{\mathbf{k}}, \end{aligned} \tag{3.29}$$

and we get the condition for the 4×4 $\mathcal{H}_k$ in the model

$$\sigma_y \mathcal{H}_{\mathbf{k}}^\star \sigma_y = \mathcal{H}_{-\mathbf{k}}. \tag{3.30}$$

Parity is implemented by switching between the two orbitals as well as inverting position and momentum; $\mathbf{k} \to -\mathbf{k}$, $\mathbf{x} \to -\mathbf{x}$. We get

$$\tau_x \mathcal{H}_{\mathbf{k}} \tau_x = \mathcal{H}_{-\mathbf{k}}. \tag{3.31}$$

We want to find a term that breaks those two conditions and also anti commutes with all other four matrices in the Hamiltonian. There is only one matrix which satisfies those conditions, τ_y. We add to our Hamiltonian a term

$$\Delta \mathcal{H}_k = m_5 \tau_y. \tag{3.32}$$

This is the symmetry breaking term we will use in the numerical calculation. We note that this is not the only way to break the symmetries.

Looking at the structure of the model

$$\Gamma_a = (\tau_z\sigma_x, \tau_z\sigma_y, \tau_z\sigma_z, \tau_x, \tau_y)\,,$$

$$d_a(\mathbf{k}) = (-2\lambda\sin k_x, -2\lambda\sin k_y, -2\lambda\sin k_z, m_{\mathbf{k}}, 0)\,,$$

we can add the following symmetry breaking terms, expanded around a Γ point

$$\Delta d_a = (m_1, m_2, m_3, 0, m_5)\,. \tag{3.33}$$

The low energy calculation suggested that the m_5 term will change the value of θ, this is not the case for m_1, m_2 and m_3. In the rest of the work we will focus on just the m_5 term.

3.3.1 Relation to field theory Lagrangian

The relation between the model and the Lagrangian used in the field theory calculation comes from the low energy behavior the model takes near the Γ points. The low energy expansion of the model have the same form at every Γ point but with different parameters

$$\mathcal{H}_{\mathbf{k},\mathbf{\Gamma}} = \sum_{\text{1}} \tau_z\sigma_i v_{\mathbf{\Gamma},i} k_i + \tau_x m_{\mathbf{\Gamma}} + \tau_y m_5, \tag{3.34}$$

where $i = x, y, z$ and

$$m_{\mathbf{\Gamma}_1} = \epsilon - 6t \ ; \ m_{\mathbf{\Gamma}_{2,3,4}} = \epsilon - 2t \ ; \ m_{\mathbf{\Gamma}_{5,6,7}} = \epsilon + 2t \ ; \ m_{\mathbf{\Gamma}_8} = \epsilon + 6t \tag{3.35}$$

are the masses at the different Γ points. The Dirac velocities are

$$v_{\mathbf{\Gamma},i} = -2\lambda\left(\cos\Gamma_x, \cos\Gamma_y, \cos\Gamma_z\right).$$

We want to use this expansion and get the parameters of the Dirac Lagrangian,

$$\mathcal{L} = \bar{\Psi}\gamma^\mu\left(i\partial_\mu - eA_\mu\right)\Psi + M\bar{\Psi}\Psi + M_5\bar{\Psi}i\gamma_5\Psi,$$

that is, we want to see what is the relation between m_5, m and the Dirac velocities from the lattice model, to M_5 and M from the Dirac Lagrangian. For this purpose we need the Hamiltonian corresponding to the Dirac Lagrangian. We use

$$\mathcal{H} = \frac{\partial \mathcal{L}}{\partial(\partial_0 \Psi)} \partial_0 \Psi + \frac{\partial \mathcal{L}}{\partial(\partial_0 \Psi^\dagger)} \partial_0 \Psi^\dagger - \mathcal{L}, \tag{3.36}$$

with

$$\begin{aligned} \frac{\partial \mathcal{L}}{\partial(\partial_0 \Psi)} &= i\Psi^\dagger \\ \frac{\partial \mathcal{L}}{\partial(\partial_0 \Psi^\dagger)} &= 0, \end{aligned} \tag{3.37}$$

to get

$$\mathcal{H} = \Psi^\dagger \left(\sum_i -i\gamma_0\gamma_i\nabla_i + M\gamma_0 + M_5 i\gamma_0\gamma_5 \right) \Psi, \tag{3.38}$$

and in momentum space

$$\mathcal{H} = \Psi^\dagger \left(\sum_i \gamma_0\gamma_i k_i + M\gamma_0 + M_5 i\gamma_0\gamma_5 \right) \Psi. \tag{3.39}$$

By changing integration variables in $\int d^3k$, we can divide the lattice Hamiltonian $\mathcal{H}_{\mathbf{k},\mathbf{\Gamma}}$ by 2λ (assuming λ is positive). For this work we are only interested in the ratio $\frac{M_5}{M}$ of the Dirac Lagrangian parameters, which does not depend on λ. This ratio is what appears in the theoretical prediction we want to test. There is one thing to be careful about, the sign of M_5 in the Dirac Lagrangian. This is not determined completely by the sign of m_5 in the lattice Hamiltonian, and in fact depends on the Dirac velocities. This comes from the fact that we need to define the matrices γ_μ in the Lagrangian differently for each Γ point

$$\gamma_\mu = \left(\tau_x, -\cos\Gamma_x \tau_x\tau_z\sigma_x, -\cos\Gamma_y \tau_x\tau_z\sigma_y, -\cos\Gamma_z \tau_x\tau_z\sigma_z\right). \tag{3.40}$$

We have

$$M_5\gamma_5 = -im_5\tau_x\tau_y = m_5\tau_z, \tag{3.41}$$

but γ_5 also needs to satisfy

$$\gamma_5 = i\gamma_0\gamma_1\gamma_2\gamma_3 = -\tau_x i\cos\Gamma_x\cos\Gamma_y\cos\Gamma_z i\tau_x\tau_z = \tau_z\cos\Gamma_x\cos\Gamma_y\cos\Gamma_z. \tag{3.42}$$

Those two equations gives the bottom line

$$M_5 = m_5\cos\Gamma_x\cos\Gamma_y\cos\Gamma_z. \tag{3.43}$$

This tells us that different Γ points will contribute to the correction to θ with a different sign for the same m_5 in the lattice model. When we look at the list of Γ points above it's easy to see that for $\mathbf{\Gamma}_1$, $M_5 = m_5$, for $\mathbf{\Gamma}_{2,3,4}$, $M_5 = -m_5$, for $\mathbf{\Gamma}_{5,6,7}$, $M_5 = m_5$ and for $\mathbf{\Gamma}_8$, $M_5 = -m_5$.

3.4 Probing θ using magneto-electric effects

To probe θ numerically we use the magneto-electric effects generated by the axion term. The magnitude of those effects depends on the value of θ, and by numerically calculating this magnitude we can extract θ.

3.4.1 m_5 domain wall

One way to probe θ is the following. We add a $\mathcal{P}$ and $\mathcal{T}$ breaking term $\sum_j \Psi_j^\dagger m_5\tau_y\Psi_j$, and we use a non-constant m_5 inside the bulk of the topological insulator. We will take $m_5(x)$ to be zero in one half of the sample and some non-zero value in the other half. We also add a constant magnetic field in the x direction $\mathbf{B} = B\hat{x}$, $\mathbf{A} = By\hat{z}$. The setup is shown in Fig 3.1.

We want to look at the charge density induced in the region where m_5 changes. We remember the formula for the charge density

$$j^0 = \rho = \frac{e^2}{4\pi^2}\nabla\theta\cdot\mathbf{B}.$$

For a single Γ point the theoretical prediction says $\theta = \text{Const}+\arctan(m_5/m)$,

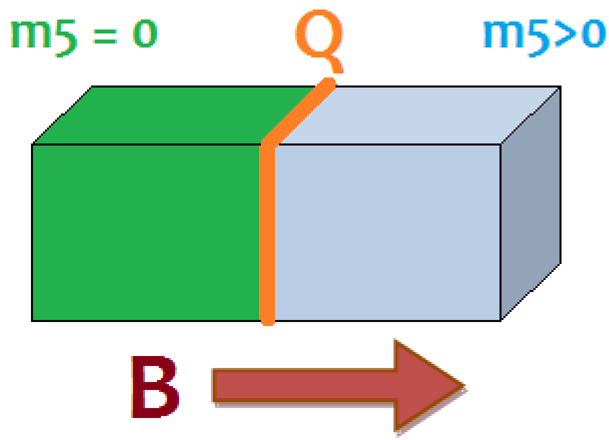

Figure 3.1: m_5 domain wall setup. $m_5 = 0$ in half of the topological insulator, and non zero in the other half. A magnetic field perpendicular to change in m_5 will result in charge accumulating on the domain wall.

where m is the mass at the Γ point. The charge we expect to get (integrated along x in the region where θ changes) is

$$Q = \int dx \rho = \frac{e^2}{4\pi^2} B \int dx \nabla_x \theta = \frac{e^2}{4\pi^2} \Delta\theta B, \tag{3.44}$$

where

$$\Delta\theta = \arctan\left(\frac{m_5}{m_0}\right) \tag{3.45}$$

is the change in θ across the domain wall.

The implementation of the magnetic field in the calculation is done using the Pierels substitution, that is, all hopping terms get a factor

$$\exp\left(i \frac{2\pi}{\Phi_0} \int_i^j \mathbf{A} \cdot \mathbf{dl}\right), \tag{3.46}$$

where the hopping is between site i and site j and

$$\Phi_0 = \frac{h}{e} = \frac{2\pi}{e} \tag{3.47}$$

is the magnetic flux quantum in natural units. Zeeman terms are not included.

For the vector potential in use, only the hopping terms in the z direction get a factor, which is the following

$$\exp\left(ieBy\right). \tag{3.48}$$

We note that the Hamiltonian remains translational invariant in the z direction after adding the varying m_5 and the magnetic field. In this case k_z remains an eigenvalue, and instead of diagonalizing the Hamiltonian for a $3D$ lattice , we are left with a k_z dependent Hamiltonian on the xy plane. We diagonalize this Hamiltonian for L_z values of $k_z \in [0, 2\pi]$ which simulates a lattice with L_z layers in the z direction. The Hamiltonian we need to diagonalize is the result of doing a Fourier transform only in the z direction, to the real space Hamiltonian. $H = \sum_{k_z} H^{k_z}$ and $H^{k_z} = H^{k_z}_{SO} + H^{k_z}_{cd} + H^{k_z}_{z}$, where

$$H^{k_z}_{SO} = i\lambda \sum_{j,\mu} \Psi^{\dagger}_{j,k_z} \tau_z \sigma_\mu \Psi_{j+\mu,k_z} + h.c \tag{3.49}$$

$$H^{k_z}_{cd} = \epsilon \sum_{j} \Psi^{\dagger}_{j,k_z} \tau_x \Psi_{j,k_z} - t \sum_{j,\mu} \Psi^{\mu}_{j,k_z} \tau_x \Psi_{j+\mu,k_z} + h.c \tag{3.50}$$

$$H^{k_z}_{z} = \sum_{j} \Psi^{\dagger}_{j,k_z} \left(-2\lambda \tau_z \sigma_z \sin\left(k_z + eBy\right) - 2t\tau_x \cos\left(k_z + eBy\right)\right) \Psi_{j,k_z} \tag{3.51}$$

$$\Delta H^{k_z} = \sum_{j} m_5(j) \Psi^{\dagger}_{j,k_z} \tau_y \Psi_{j,k_z}. \tag{3.52}$$

$\mu = x, y$ and j is only in the xy plane.

If we work with a $L \times L$ lattice on the xy plane, then for each k_z we have a $4L^2 \times 4L^2$ Hamiltonian. We diagonalize and get the eigenvectors ψ_{n,k_z}, $n = 1 \ldots 4L^2$. For half filling we take the $2L^2$ eigenvectors with the negative eigenvalues. This is due to our expectation that for small perturbations (small m_5 and B) we still get two negative and two positive bands like in the original Hamiltonian, and for each k_z separately half the eigenvalues will be negative and half will be positive. The charge density is calculated from

$$\rho(x,y) = \sum_{n,k_z,l} \left(\left|\psi_{n,k_z}(x,y,l)\right|^2 - \frac{1}{2} \right). \tag{3.53}$$

$l = 1, 2, 3, 4$ is for summing over the orbitals and the spins. The $-\frac{1}{2}$ is due to the fact that we want to see the change from the situation with no magnetic field and no m_5, in which we have two electrons in each site (at half filling).

We have open boundary conditions on the y axis, that is, the sites at $y = 0$ and $y = L$ do not have hopping terms to their left and right respectively. We must use open boundary conditions on the y axis due to the vector potential dependence on y. For the x axis we can use either open or periodic boundary conditions. For periodic boundary conditions we have hopping terms between the sites at $x = 0$ and the sites at $x = L$.

For the x axis we expect different charge distribution depending on the boundary conditions. For open boundary conditions, the surfaces at $x = 0$ and $x = L$ are surfaces between topological insulator and vacuum so there should be charge accumulated there corresponding to the jump in θ, from the value it takes inside the topological insulator, π plus a correction due to m_5, and $\theta = 0$ in the vacuum. For periodic boundary conditions, the jump in θ can only come from different m_5 between the $x = 0$ surface and the $x = L$ surface.

3.4.2 Flux insertion

A different setup that allows a calculation of θ is the flux insertion. Following ref [23] we consider a topological insulator with a thin tube carrying magnetic flux. The topological insulator is coated by a magnetic film that breaks time reversal on the surface, in order to create a gap for the surface states. The setup is shown in the Fig. 3.2, taken from ref [23]. In this setup, charge with a magnitude proportional to the value of θ will be accumulated on the surface of the topological insulator, in the vicinity of the flux tube.

We consider the magnetic flux inside the tube being raised from 0 to some value $\eta\Phi_0 = \eta\frac{2\pi}{e}$. We use Faraday's law to get the electric field in

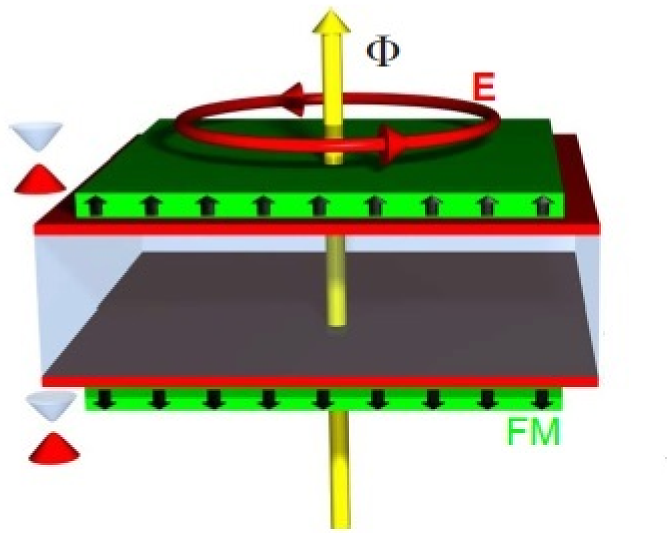

Figure 3.2: Flux insertion setup diagram, from ref. [23]. On the top and bottom surfaces of the topological insulator we have ferromagnetic coating. The yellow arrow is the magnetic flux, the red arrow illustrates the electric field generated when the magnetic flux is raised from zero.

cylindrical coordinates (ρ, ϕ, z), and take the magnetic field to be in the z direction

$$\begin{aligned} &\nabla \times \mathbf{E} = -\frac{\partial \mathbf{B}}{\partial t} \rightarrow \\ &\frac{1}{\rho}\frac{\partial(\rho E_\phi)}{\partial \rho} = -\frac{\partial B_z}{\partial t}, \end{aligned} \tag{3.54}$$

and

$$E_\phi(\rho) = -\frac{\partial B_z}{\partial t}\frac{R^2}{2\rho}, \tag{3.55}$$

where R is the radius of the tube. On the z surfaces of the topological insulator we have Hall conductance $\sigma_{xy} = \frac{e^2}{4\pi}$, due to the magnetic coating that opens a gap on the surface. This result follows from the electromagnetic action discussed in the introduction, and also from the microscopic description

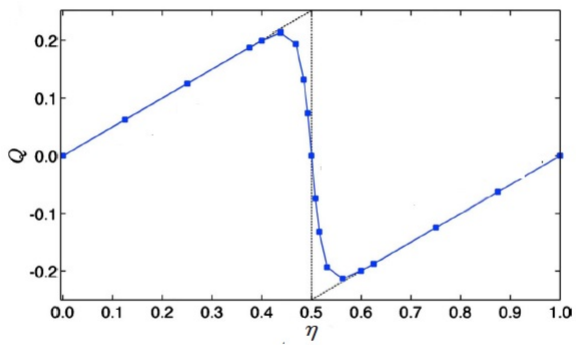

Figure 3.3: Charge accumulated on the flux tube Vs. the magnetic flux, from ref. [23]. The setup is shown in Fig. 3.2. The magnetic flux in the tube is $\Phi = \eta\Phi_0$, when Φ_0 is the magnetic flux quantum.

of the surface state (ref. [12]). The Hall conductance creates a current

$$j_\rho(\rho) = \frac{e^2}{4\pi}E_\phi(\rho) = -\sigma_{xy}\frac{\partial B_z}{\partial t}\frac{R^2}{2\rho}. \tag{3.56}$$

The magnetic field is $B_z(t) = \frac{\Phi(t)}{\pi R^2}$. The charge accumulated near the flux tube is

$$\begin{aligned} Q = \int_0^T dt \int_0^{2\pi} \rho d\phi\, j_\rho(\rho) &= \int_0^T dt \int_0^{2\pi} \rho d\phi \frac{\partial \Phi(t)}{\partial t}\sigma_{xy}\frac{1}{2\pi\rho} \\ &= \eta\Phi_0\sigma_{xy} = \eta\frac{2\pi}{e}\frac{e^2}{4\pi} = \eta\frac{e}{2}. \end{aligned} \tag{3.57}$$

This is the charge in the case of a $\mathcal{T}$ and $\mathcal{P}$ invariant topological insulator, where $\theta = \pi$. In our case, when θ is not quantized at π we will have a different hall conductance $\sigma_{xy} = \frac{\theta e^2}{4\pi^2}$ and the charge will be

$$Q = \eta e\frac{\theta}{2\pi}. \tag{3.58}$$

In order to use this setup we set η in the range between 0 and 0.5. From ref [23], the dependence of the charge on η is shown in Fig. 3.3.

For $\eta = 1$ we expect to get $Q = 0$, as an integer flux quantum can be removed by a gauge transformation. The effect at $\eta = 0.5$, called the wormhole effect, is the topic of ref [23]. They find that the flux tube turns conducting for this value of η. A value of θ different than π is expected to keep the overall shape the same, but change the slope of the lines between 0 and 0.5, and between 0.5 and 1.

The vector potential needed for the Pierels substitution in the lattice model for this setup is $\mathbf{A} = A_\phi \hat{\phi}$ with

$$\begin{aligned} A_\phi &= \frac{\eta \Phi_0 \rho}{2\pi R^2} \qquad\qquad \rho < R \\ A_\phi &= \frac{\eta \Phi_0}{2\pi R} \qquad\qquad \rho > R. \end{aligned} \tag{3.59}$$

We consider a very thin tube for which all the sites are outside of the tube.

In this setup we need a $\mathcal{T}$ breaking term on the surface. For the i surface we add the following term to the Hamiltonian,

$$\Delta H_{S_i} = \Omega \sum_{j \in i-\mathrm{surf}} \Psi_j^\dagger \sigma_i \Psi_j, \tag{3.60}$$

where Ω is the strength of the surface magnetization.

We use open boundary conditions on the z axis and can use either open or periodic boundary conditions on the x and y axes. For periodic boundary conditions on x and y we put additional flux tubes in the locations $n_x L\hat{x} + n_y L\hat{y}$ from the original tube, n_x, n_y being integers. This is necessary in order to make the system periodic.

3.4.3 Magnetic monopole

In this setup we place a magnetic monopole inside a topological insulator, following ref. [21]. With this setup we have what is called the Witten effect (ref [22]). A charge with a magnitude proportional to θ is accumulated close to the magnetic monopole.

To see the effect of the magnetic monopole we look at Maxwell's equations in presence of the axion term. A non zero axion term will add extra terms to Gauss' law and to Ampere's law

$$
\begin{aligned}
\nabla \cdot \mathbf{E} &= \rho - \frac{e^2}{4\pi^2}\nabla\theta \cdot \mathbf{B} \\
\nabla \times \mathbf{B} &= \frac{\partial \mathbf{E}}{\partial t} + \mathbf{j} + \frac{e^2}{4\pi^2}\left(\nabla\theta \times \mathbf{E} + \frac{\partial\theta}{\partial t}\mathbf{B}\right),
\end{aligned}
$$

where ρ and $\mathbf{j}$ are the electric charge density and electric current. The two other equations remain unchanged. For a unit magnetic monopole at the origin we have

$$
\begin{aligned}
\nabla \cdot \mathbf{B} &= \Phi_0 \delta(\mathbf{r}) \\
\mathbf{B} &= \frac{\Phi_0}{4\pi r^2}\hat{r}.
\end{aligned} \tag{3.61}
$$

The divergence of the magnetic field at the origin will destroy the topological order there and we will have $\theta(\mathbf{r}=0)=0$. Further away from the magnetic monopole the original value of θ will be restored. We think of θ as a function of the radius with $\theta(\mathbf{r}=0)=0$ and $\theta(\mathbf{r}=R)=\pi$ for large enough R. We do a volume integration of the second term on the right hand side of the modified Gauss' law, to get an effective electric charge bound to the magnetic monopole

$$
\begin{aligned}
Q &= -4\pi \int_0^R r^2 \frac{e^2}{4\pi^2}\frac{\partial\theta}{\partial r}\frac{\Phi_0}{4\pi r^2} \\
&= -\frac{e^2\Phi_0}{4\pi^2}\int_0^R \frac{\partial\theta}{\partial r} \\
&= -\frac{e}{2}\pi.
\end{aligned} \tag{3.62}
$$

In our case, when the symmetries are broken and originally inside the topological insulator $\theta \neq \pi$ we have $Q = -\frac{\theta}{2\pi}e$.

For the Pierels substitution, the vector potential used in the lattice model is (where (θ, ϕ) are the spherical angles)

$$
\mathbf{A} = -\Phi_0(1+\cos\theta)\nabla\phi. \tag{3.63}
$$

3.4.4 Usage of $\frac{\pi}{4}$ rotation symmetry in the numerical calculation

In both the flux insertion and the magnetic monopole setups we have a $\frac{\pi}{4}$ rotation symmetry around the z axis. We can use the symmetry to make the exact diagonalization procedure more efficient. We note that in both cases we choose the vector potential to respect this symmetry. We start with a L^3 lattice and $(4L^3) \times (4L^3)$ Hamiltonian. Using the symmetry we block diagonalize the Hamiltonian into four $L^3 \times L^3$ parts. The diagonalization of those four $L^3 \times L^3$ matrices is faster then one $(4L^3) \times (4L^3)$ matrix and allows us to use larger values of L.

This is done by writing the Hamiltonian in the basis of eigenstates of the $\frac{\pi}{4}$ rotation operator. The $\frac{\pi}{4}$ rotation operator mixes the sites in groups of four. In each of those groups, starting from one site, one can get to the other three by consequent rotations of $\frac{\pi}{4}$ around the z axis. In the subspace of only one of those groups, we can write the operator

$$\begin{pmatrix} 0 & 1 & 0 & 0 \\ 0 & 0 & 1 & 0 \\ 0 & 0 & 0 & 1 \\ 1 & 0 & 0 & 0 \end{pmatrix}. \tag{3.64}$$

We can think of the 1's as being $1_{4\times 4}$ in orbital and spin space. For each eigenstate of the matrix above we construct $4\frac{L}{4} \times L \times L$ eigenstates of the full $\frac{\pi}{4}$ rotation operator.

As this is a unitary operator that commutes with the Hamiltonian, eigenstates with different eigenvalues will have zero Hamiltonian matrix element, and so when we write the Hamiltonian in this new basis it will be block diagonal.

Even after exploiting the symmetry to make the calculation more efficient, the flux tube and magnetic monopole setups remain much slower than the m_5 domain wall. For this reason we will mostly work with the m_5 domain wall setup, and use the other two to confirm the results.

3.5 Physical interpretation of non zero m_5

As discussed, topological insulators can be described by the theory of a single Dirac fermion. That is, by the Lagrangian

$$\mathcal{L} = \bar{\Psi}\gamma^{\mu}\left(i\partial_{\mu} - eA_{\mu}\right)\Psi + m\bar{\Psi}\Psi.$$

When we add a m_5 term to this low energy theory we get the same result for θ for any topological insulator model considered. But for different models, the physical interpretation of the m_5 term can be different. For the lattice model in use here we have

$$\Delta\mathcal{H}_k = m_5\tau_y,$$

where τ_y is in orbital space. While in this case the interpretation of the symmetry breaking term is not clear, in other topological insulator models, that do describe real solids, there is a physical interpretation. In ref. [18] can be found a discussion regarding the physical interpretation of a m_5 term, for a lattice model describing the low energy bands of the topological insulators Bi_2Te_3, Bi_2Se_3 and Sb_2Te_3. They find that the m_5 term represents in this case a staggered Zeeman field, pointing in the opposite direction for the two sub-lattices in their model. What can create such a Zeeman field is anti-ferromagnetic order.

Chapter 4

Calculation of the θ parameter from band structure

We can get the value for θ in the model with the $\mathcal{P}$ and $\mathcal{T}$ breaking term in another way. To get the topological phases of the model without the symmetry breaking term we used the band structure formula for θ

$$\theta = \frac{1}{4\pi}\int_{BZ} d^3k\epsilon^{ijk}\ \mathrm{Tr}\left[A_i\partial_j A_k + i\frac{2}{3}A_iA_jA_k\right].$$

We want to do a similar calculation to see what is the effect of breaking $\mathcal{P}$ and $\mathcal{T}$. We can use the results from ref. [1] and ref. [18], for a Dirac Hamiltonian of the form

$$\mathcal{H}_{\mathbf{k}} = \sum_{a=1}^{5}\Gamma_a d_a(\mathbf{k}),$$

where Γ_a are anti commuting matrices. In this case we have

$$\frac{\partial\theta(\xi)}{\partial\xi} = \frac{3}{4\pi}\int d^3k\frac{1}{|d|^5}\epsilon^{abcde}d_a\partial_{k_z}d_b\partial_{k_y}d_c\partial_{k_x}d_d\partial_\xi d_e. \tag{4.1}$$

where ξ is some parameter in the Hamiltonian. We remember that for the model used in this work we have

$$\Gamma_a = (\tau_z\sigma_x, \tau_z\sigma_y, \tau_z\sigma_z, \tau_x, \tau_y)$$

$$d_a(\mathbf{k}) = (-2\lambda \sin k_x, -2\lambda \sin k_y, -2\lambda \sin k_z, m_{\mathbf{k}}, m_5)\,.$$

This result is obtained by first calculating the Chern number for a Dirac Hamiltonian in $4+1$ dimensions (ref. [1], equation (64))

$$C_2 = \frac{3}{8\pi^2}\int d^4\mathcal{K}\epsilon^{abcde}\frac{d_a\partial_{\mathcal{K}_z}d_b\partial_{\mathcal{K}_y}d_c\partial_{\mathcal{K}_x}d_d\partial_{\mathcal{K}_w}d_e}{|d(\mathcal{K})|^5}. \tag{4.2}$$

The physical meaning of the Chern number is of less importance here. The Chern number was also shown to be (ref. [1], equation (54))

$$C_2 = \frac{1}{32\pi^2}\int d^4\mathcal{K}\epsilon^{ijkl}\mathrm{Tr}[F_{ij}F_{kl}], \tag{4.3}$$

where

$$F_{ij} = \partial_i A_j - \partial_j A_i, \tag{4.4}$$

and

$$A_i^{\alpha\beta} = -i < \alpha\,\mathcal{K}\,|\frac{\partial}{\partial\mathcal{K}_i}|\,\beta\,\mathcal{K} >. \tag{4.5}$$

$|\,\beta\,\mathcal{K} >$ is the β eigenstate of $\mathcal{H}_{\mathcal{K}}$. Here $\mathcal{K} = (\mathcal{K}_x, \mathcal{K}_y, \mathcal{K}_z, \mathcal{K}_w)$ is a four dimensional vector. A dimensional reduction from $4+1$ to $3+1$ dimensions can be performed by taking the momentum in the extra dimension, $\mathcal{K}_w$, to be a parameter. We denote this parameter with ξ. From the results of the dimensional reduction we see (ref. [1], equation (76))

$$\frac{\partial\theta(\xi)}{\partial\xi} = \frac{1}{4\pi}\int d^3k\epsilon^{ijk}\mathrm{Tr}[F_{\xi i}F_{jk}]. \tag{4.6}$$

When this is compared to the Chern number formulas, we get the result for $\frac{\partial\theta(\xi)}{\partial\xi}$ in terms of the Hamiltonian parameters

$$\frac{\partial\theta(\xi)}{\partial\xi} = \frac{3}{4\pi}\int d^3k \frac{1}{|d(\mathbf{k})|^5}\epsilon^{abcde} d_a \partial_{k_z} d_b \partial_{k_y} d_c \partial_{k_x} d_d \partial_\xi d_e. \tag{4.7}$$

The next step is to get a formula for θ, we follow Ref. [18]. We look at the following parameterization

$$d_a(\mathbf{k},\lambda) = (d_1(\mathbf{k}), d_2(\mathbf{k}), d_3(\mathbf{k}), d_4(\mathbf{k}) + \xi, d_5(\mathbf{k}))\,. \tag{4.8}$$

The special role of d_4 here comes from the fact that Γ_4 is the only $\mathcal{P}$ and $\mathcal{T}$ invariant matrix in the Hamiltonian, the $a = 1,2,3$ terms are only invariant with the $\sin k$ factors. In any Dirac Hamiltonian we will have only one matrix that is invariant under $\mathcal{P}$ and $\mathcal{T}$ (ref. [25]). With this parameterization we have

$$\frac{\partial\theta(\xi)}{\partial\xi} = \frac{3}{4\pi}\int d^3k \epsilon^{abcd4} \frac{d_a \partial_{k_z} d_b \partial_{k_y} d_c \partial_{k_x} d_d}{\left(|d_{\xi=0}|^2 - d_4^2 + (d_4+\xi)^2\right)^{\frac{5}{2}}}, \tag{4.9}$$

and

$$\theta(\xi = 0) = \theta(\xi = \infty) - \int_0^\infty d\xi \frac{\partial\theta(\xi)}{\partial\xi}. \tag{4.10}$$

First we look at the constant $\theta(\xi = \infty)$. The Hamiltonian at $\xi = \infty$ is

$$H(\xi \to \infty) = \xi\Gamma_4. \tag{4.11}$$

Thanks to the specific choice of parameterization we get a Hamiltonian that is $\mathcal{T}$ symmetric and clearly topologically trivial, so we have $\theta(\xi = \infty) = 0$. Next we evaluate the integral

$$\int_0^\infty d\xi \frac{3}{4\pi}\int d^3k \epsilon^{abcd4} \frac{1}{\left(|d_{\xi=0}|^2 - d_4^2 + (d_4+\xi)^2\right)^{\frac{5}{2}}} d_a \partial_{k_z} d_b \partial_{k_y} d_c \partial_{k_x} d_d. \tag{4.12}$$

We use

$$
\begin{aligned}
&\int_0^\infty dx \frac{1}{(a^2-b^2+(b+x)^2)^{\frac{5}{2}}} \\
&= \left.\frac{(b+x)(3a^2-b^2+4bx+2x^2)}{3(a^2-b^2)^2(a^2+x(2b+x))^{\frac{3}{2}}}\right|_{x=0}^{x=\infty} \\
&= \frac{2}{3(a^2-b^2)^2} - \frac{b(3a^2-b^2)}{3(a^2-b^2)^2a^3} \\
&= \frac{b(b^2-2ab+a^2)-4a^2b+2a^3+2ab^2}{3(a-b)^2(a+b)^2a^3} \\
&= \frac{2a+b}{3(a+b)^2a^3},
\end{aligned}
\tag{4.13}
$$

and get the formula for θ for Dirac Hamiltonians with non zero d_5

$$
\theta = \frac{1}{4\pi}\int_{BZ} d^3k \frac{2|d|+d_4}{\left(|d|+d_4\right)^2|d|^3}\epsilon^{ijkl} d_i\partial_{k_x}d_j\partial_{k_y}d_k\partial_{k_z}d_l, \tag{4.14}
$$

where $i,j,k,l = 1,2,3,5$. We evaluate the integral twice. First we look at the contribution from momenta close to the Γ points, this could be done explicitly. We also evaluate the entire integral numerically.

4.1 Low energy contribution

For a single Γ point we have

$$
d^a(\mathbf{\Gamma}) = \left(v_{x,\mathbf{\Gamma}}k_x, v_{y,\mathbf{\Gamma}}k_y, v_{z,\mathbf{\Gamma}}k_z, m_{\mathbf{\Gamma}}, m_5\right),
$$

and we can write

$$
\epsilon^{ijkl} d_i\partial_{k_x}d_j\partial_{k_y}d_k\partial_{k_z}d_l = m_5 v_{x,\mathbf{\Gamma}}v_{y,\mathbf{\Gamma}}v_{z,\mathbf{\Gamma}}. \tag{4.15}
$$

We take the integration limits to cover the entire k space (which is the same as field theory calculations). In this case we can get rid of the -2λ factors in the Dirac velocities by changing variables $k_i \to -2\lambda k_i$. This gives an overall minus sign from changing ∞ to $-\infty$ in the integration limits for each k_i. In the end of the day we have an overall sign factor coming from the Dirac velocities $-\mathrm{sgn}\,(v_{x,\mathbf{\Gamma}}v_{y,\mathbf{\Gamma}}v_{z,\mathbf{\Gamma}})$. Without writing this factor we have

$$\theta_{\mathbf{\Gamma}} = m_5 \int_0^\infty dk k^2 \frac{2\sqrt{k^2+m_0^2+m_5^2}+m_0}{\left(\sqrt{k^2+m_0^2+m_5^2}+m_0\right)^2 \sqrt{k^2+m_0^2+m_5^2}^3}, \tag{4.16}$$

where this is after the integration over $d\Omega$. This is the contribution from one Γ point, and $m_0 = m_{\mathbf{\Gamma}}$. We write

$$m = m_0 + im_5, \tag{4.17}$$

and

$$m = |m| \exp i\beta. \tag{4.18}$$

We can change integration variables,

$$\tan\alpha = \frac{k}{|m|}, \tag{4.19}$$

to get

$$\begin{aligned} \theta = \sin\beta \int_0^{\frac{\pi}{2}} d\alpha \frac{2\sqrt{\tan^2\alpha+1}+\cos\beta}{\left(\sqrt{\tan^2\alpha+1}+\cos\beta\right)^2 \sqrt{\tan^2\alpha+1}^3} \frac{\tan^2\alpha}{\cos^2\alpha} \\ = \sin\beta \int_0^{\frac{\pi}{2}} d\alpha \frac{2+\cos\alpha\cos\beta}{(1+\cos\alpha\cos\beta)^2} \sin^2\alpha. \end{aligned} \tag{4.20}$$

This integral gives

$$\begin{aligned} \sin\beta \left[\frac{2\arctan\left(\frac{(\cos\beta-1)\tan\frac{\alpha}{2}}{\sqrt{1-\cos^2\beta}}\right)}{\sqrt{1-\cos^2\beta}} - \frac{\sin\alpha\cos\alpha}{\cos\beta\cos\alpha+1} \right] \Bigg|_{\alpha=0}^{\alpha=\frac{\pi}{2}} \\ = 2\arctan\left(\frac{\cos\beta-1}{\sin\beta}\right) = 2\arctan\left(\frac{-2\sin^2\frac{\beta}{2}}{2\sin\frac{\beta}{2}\cos\frac{\beta}{2}}\right) = -\beta, \end{aligned} \tag{4.21}$$

and the final result is

$$\Delta\theta_{\mathbf{\Gamma}} = \beta_{\mathbf{\Gamma}}\,\mathrm{sgn}\,(v_{x,\mathbf{\Gamma}}v_{y,\mathbf{\Gamma}}v_{z,\mathbf{\Gamma}})\,. \tag{4.22}$$

That is, the contribution to θ coming from each Γ point is the phase of the complex mass $m = m_0 + im_5$ at the Γ point, with a sign determined by the Dirac velocities.

4.2 Full Brillouin zone contribution

We want to check whether or not there is a contribution from momenta far from the Γ points. To do this we can evaluate the entire θ integral numerically. We use a 3D grid for k_x, k_y, k_z and evaluate

$$\theta = \frac{-2\lambda^3}{\pi} \int_{BZ} d^3k \frac{2\sqrt{-2\lambda \sum_{i=x,y,z} \sin {k_i}^2 + m_{\mathbf{k}}^2 + m_5^2} + m_{\mathbf{k}}^2}{\left(\sqrt{\cdots} + m_{\mathbf{k}}^2\right)^2 \sqrt{\cdots}^3} \times \\ m_5 \cos k_x \cos k_y \cos k_z, \tag{4.23}$$

where $m_{\mathbf{k}} = \epsilon - 2t \sum_{i=x,y,z} \cos k_i$ and in this case m_5 is constant.

Chapter 5

Results

5.1 m_5 domain wall

We start with the m_5 setup shown in Fig. 3.1, for which $m_5 = 0$ on half the sample and takes some non zero value on the other half. The charge density calculated numerically for this setup generally have a shape as shown in Fig. 5.1.

We note that the charge density on edges of the sample in the x direction is expected as θ jumps there from π (up to a correction of order $\frac{m_5}{m_0}$) to 0. The different sign on the two edges is due to different relative direction between the jump of θ and the magnetic field. The charge accumulated on the edges of the sample in the y direction is explained by the fact that this surface is conducting.

We are interested in the charge accumulated due to the jump in m_5. To get this charge we sum over the charge density across the domain wall for a specific y

$$Q = \sum_x \rho(x, y). \tag{5.1}$$

The range of x over which we sum depends on the sample size and the m_5 profile in use. It is determined by looking at the charge density distribution, and by comparing the result obtained with different ranges to the theoretical prediction. The result for this charge is reliable only if it does not vary

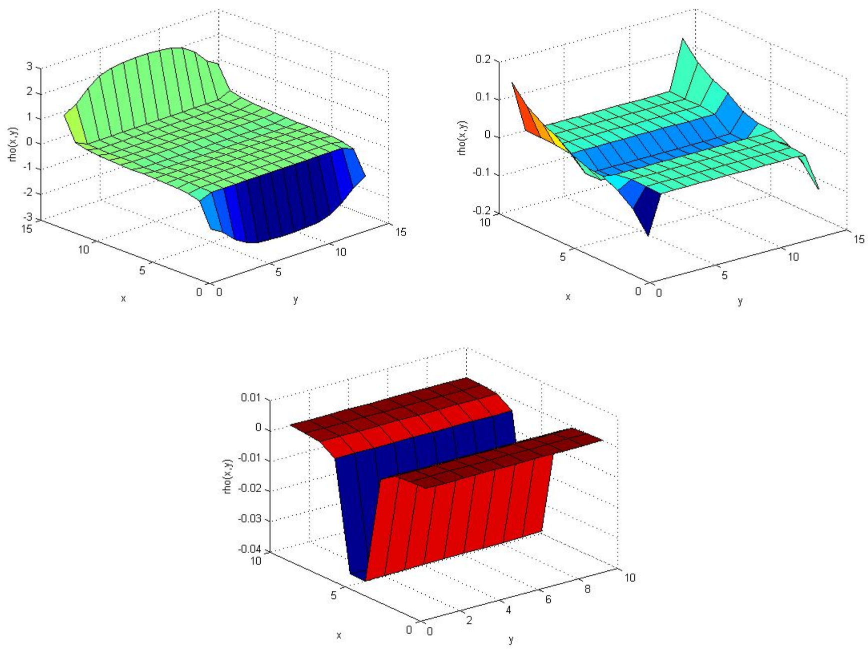

Figure 5.1: Three images of the charge distribution for the m_5 domain wall setup. All three images are of the same charge density. The first one (top left) is of the entire 14×14 xy plane, the second one (top right) is of the entire sample in the y direction but without the edges on the x direction. The third image (bottom) is without the edges on both axes. Without edges means without two sites on each edge. We are mainly interested in the third image in which we can see clearly the charge density due to the jump in m_5. $m_5 = 0.05$ on half the sample and $m_5 = 0$ on the other half, $L = 14$ and we use open boundary conditions on both the x and y axes. Other model parameters are $\frac{2\pi a^2}{\Phi_0} B = eB = 0.2$ ($a = 1$ is the lattice constant), $t = \lambda = 1$, $\epsilon = 4$, $L_z = 160$.

significantly when we change the x range by $1-2$ lattice sites. In this case we can be sure that there is no overlap between the charge on the m_5 domain wall and the charge on the topological insulator surface. We do this sum for a y value at the center of the sample. Again, a reliable result does not vary significantly with y.

We present the results in terms of $\Delta\theta$ instead of charge

$$\Delta\theta = \frac{4\pi^2}{L_z B} Q. \tag{5.2}$$

This is coming from the axion charge density formula

$$\rho = \frac{1}{4\pi^2} \Delta\theta B.$$

The factor of L_z is because L_z values of k_z corresponds to a lattice with L_z sites along the z direction. Our result for the charge density on the xy plane is effectively the sum of the charge density along z.

We will look at the dependence of $\Delta\theta$ on the masses at the Γ points. For the eight Γ points in our model the masses are

$$m_1 = \epsilon - 6t \ ; \ m_{2,3,4} = \epsilon - 2t \ ; \ m_{5,6,7} = \epsilon + 2t \ ; \ m_8 = \epsilon + 6t.$$

We control these masses by changing ϵ. Fig. 5.2 is showing the numerical results for $\Delta\theta$, for different values of ϵ.

The theoretical prediction is that each Γ point will contribute $\pm \arctan\left(\frac{m_5}{m_0}\right)$ to θ, where m_0 is the mass at the Γ point. The sign is determined by the Dirac velocities at the Γ point. The prediction for $\Delta\theta$ due to $\mathcal{P}$ and $\mathcal{T}$ breaking m_5 is

$$\begin{aligned}\Delta\theta = &- \arctan\left(\frac{m_5}{\epsilon+6}\right) + 3\arctan\left(\frac{m_5}{\epsilon+2}\right) \\ &- 3\arctan\left(\frac{m_5}{\epsilon-2}\right) + \arctan\left(\frac{m_5}{\epsilon-6}\right).\end{aligned} \tag{5.3}$$

For $m_5 = 0.05$ this theoretical prediction is shown in Fig. 5.3. Next we want to compare the numerical data to the theoretical prediction. This is

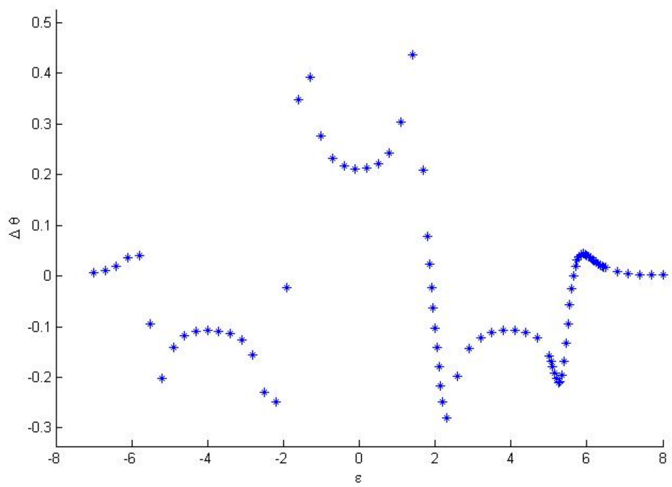

Figure 5.2: Numerical results for the change in θ due to a non zero m_5 Vs. ϵ. ϵ controls the masses at the Γ points. $m_5 = 0.05$. In this case $L_z = 100$, all other parameters are the same as before ($eB = 0.2$, $m_5 = 0.05$, $t = \lambda = 1$, $L = 14$ in the rest of the work we use $t = \lambda = 1$, $L = 14$ unless stated otherwise).

done in Fig. 5.4.

We see that the general features are similar but the agreement is not exact. It is clear that there is a correction to the value of θ due to m_5 and it looks like the theoretical formula is a good prediction for this correction.

At the values of ϵ in which the gap closes for one or more of the Γ points, we do not expect to get good results from the numerical calculation. The reason is that when the gap is small there is a problem with the localization of the charge on the domain wall. This can be seen in Fig. 5.5. Here $\epsilon = 5.4$, other parameters are the same as in the image of the charge density for $\epsilon = 4$ shown in Fig. 5.1. We see that the charge that was localized on the surface before is now spread out on the sample. The charge on the m_5 domain wall is hard to see here.

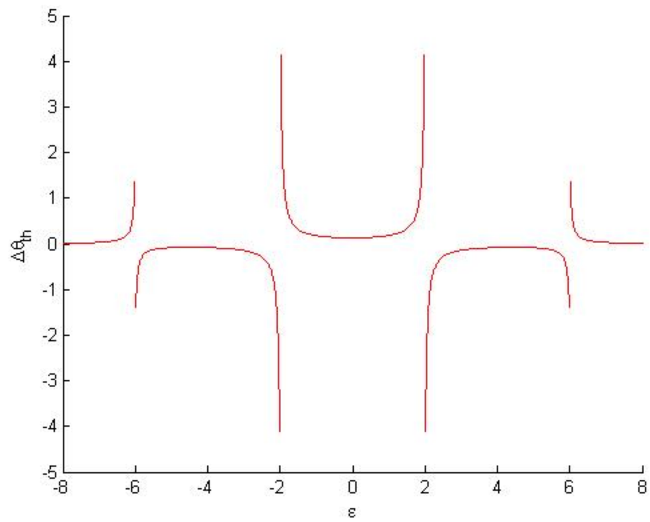

Figure 5.3: Theoretical prediction for the change in θ due to a non zero m_5 Vs. ϵ which controls the masses at the Γ points. $m_5 = 0.05$.

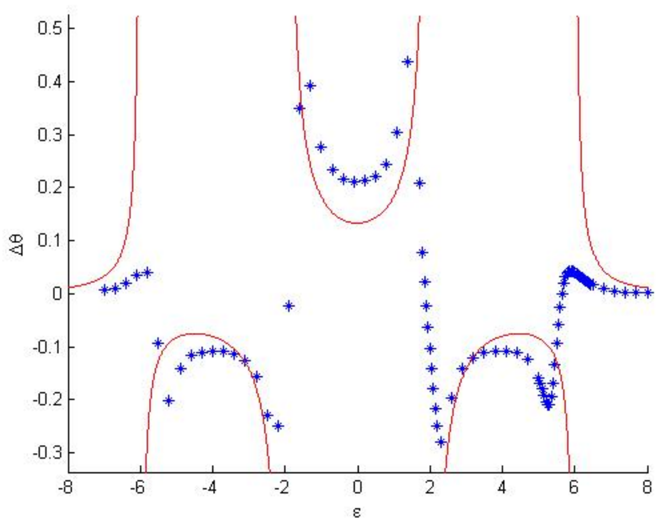

Figure 5.4: Comparison between the theoretical prediction and the numerical results. $m_5 = 0.05$.

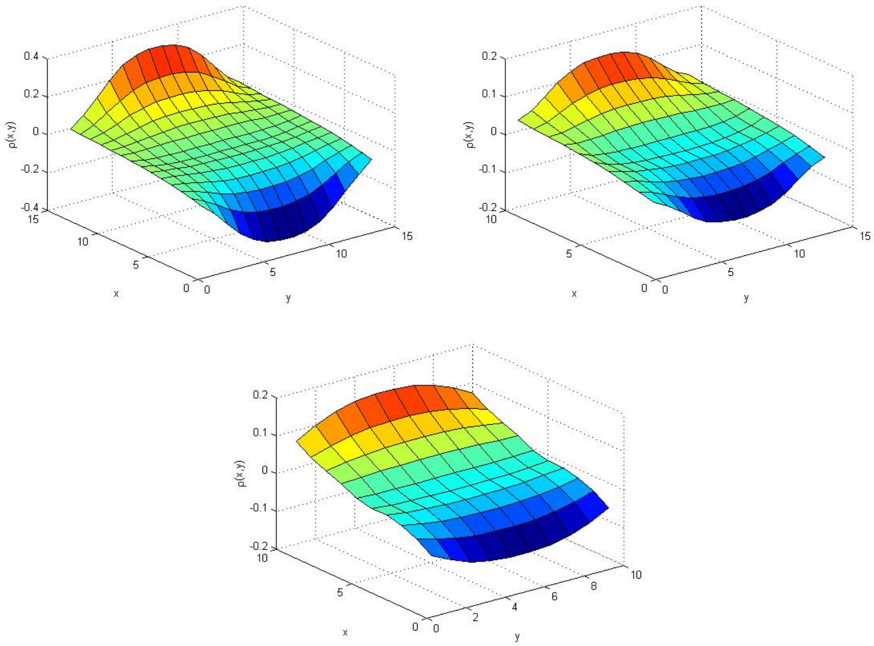

Figure 5.5: Charge distribution for the m_5 domain wall setup, for the case of small band gap. In this case the charge is not localized on the domain wall. To be compared with Fig. 5.1

We want to find the cause of the discrepancy between the theoretical and the numerical result for values of ϵ in which the gap is large, to do this we turn to the band structure evaluation of θ.

5.2 θ from band structure

When we use band structure formulas to evaluate θ we get the following integral

$$\theta = \frac{-2\lambda^3}{\pi} \int_{BZ} d^3k \frac{2\sqrt{-2\lambda \sum_{i=x,y,z} \sin {k_i}^2 + m_{\mathbf{k}}^2 + m_5^2} + m_{\mathbf{k}}^2}{\left(\sqrt{\cdots} + m_{\mathbf{k}}^2\right)^2 \sqrt{\cdots}^3}$$
$$m_5 \cos k_x \cos k_y \cos k_z .$$

$m_{\mathbf{k}} = \epsilon - 2t\sum_{i=x,y,z} \cos k_i$. We saw that the low energy contribution to this integral is the same as the field theory prediction. Here we look at the numerical evaluation of the full Brillouin zone integral. In Fig. 5.6 we compare the full Brillouin zone prediction, the low energy prediction, and the results from the lattice model. For a range of ϵ we calculate both predictions for $\Delta\theta$, the difference in θ between the case with $m_5 = 0.05$ and the case with $m_5 = 0$. For the lattice model what is shown is the jump in θ on a surface between $m_5 = 0$ and $m_5 = 0.05$. That is, the results from the previous section.

We see that other than in the vicinity of $\epsilon = 6$ and $\epsilon = 2$ there is an exact agreement between the lattice model and the full Brillouin zone prediction, as expected. We see that there is a deviation from the low energy prediction. The fact that we see the same deviation in two different calculations suggests that it is a real deviation and that the low energy should be thought of as an approximation.

We can also look at the dependence of the full θ on m_5. For the lattice model result, to get the full θ, we add π to the $\Delta\theta$ we get from the numerical calculation. This is done in Fig. 5.7. Again we see a good agreement between the full Brillouin zone prediction to the lattice calculation with a deviation from the low energy prediction.

We conclude that the low energy prediction, is an approximation to the form θ takes in the presence of an $im_5\gamma_5$ term. In the next section we present more results obtained also from the flux insertion and monopole setup to confirm this conclusion.

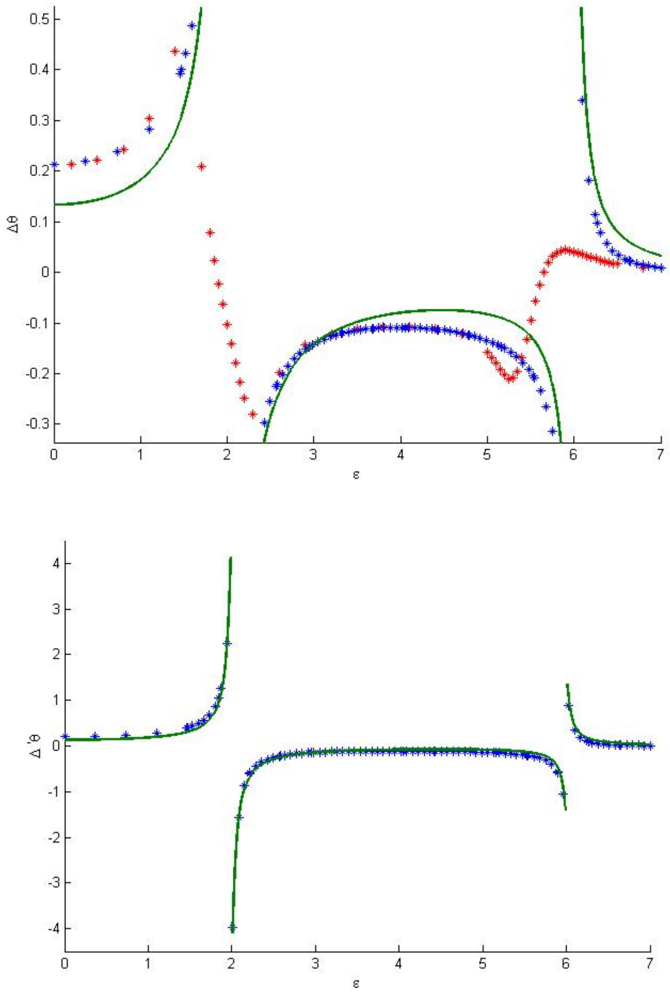

Figure 5.6: $\Delta\theta$ Vs. ϵ, Comparison between the numerical results and the low energy and full Brillouin zone predictions. Numerical results in red, low energy prediction in green, full Brillouin zone prediction in blue. $m_5 = 0.05$. $\Delta\theta$ is the difference in θ between the case with $m_5 = 0.05$ and the case with $m_5 = 0$. Bottom figure is zoomed out.

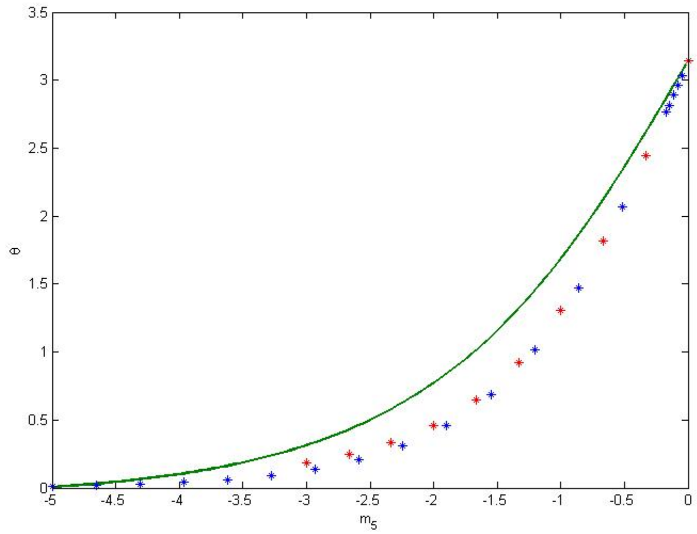

Figure 5.7: θ Vs. m_5, Low energy prediction in green, full Brillouin zone prediction in blue, lattice model results in red. $\epsilon = 4$.

5.3 Comparison of different numerical calculations

In order to make sure that the deviation of the numerical result in the m_5 domain wall setup from the low energy prediction is not a numerical error, we compare it to results from the magnetic monopole and flux insertion setups. We also try a gradual m_5 domain wall. This is in order to check if the deviation from the low energy prediction, seen in the last section, is a result of the abrupt change in m_5 in the original m_5 domain wall setup.

First we try gradual domain wall and periodic boundary conditions, in the m_5 domain wall setup. We use the following m_5 profile

$$m_5(x) = \frac{1}{2} m_5 \left(\tanh\left(\frac{x - \frac{L}{4}}{\xi} \right) - \tanh\left(\frac{x - \frac{3L}{4}}{\xi} \right) \right). \tag{5.4}$$

We calculate the charge density and the charge accumulated on the domain wall for $\xi = 1, 2, 3$. The charge density in this setup is shown in Fig. 5.8.

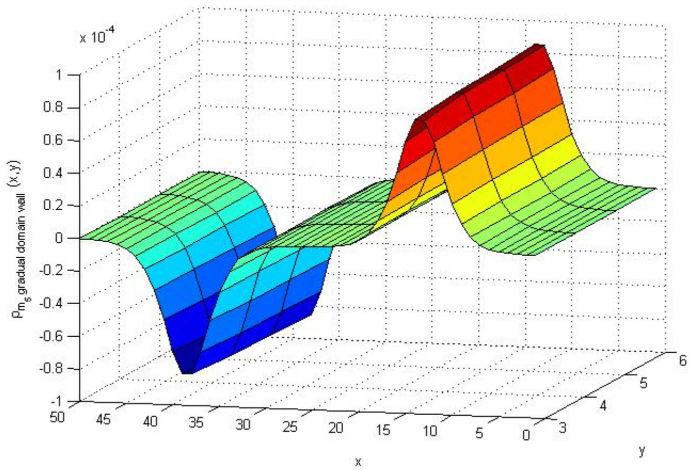

Figure 5.8: Charge density for the m_5 domain wall setup, using a gradual domain wall in which m_5 changes gradually from $m_5 = 0$ on the surfaces to $m_5 = 0.1$ in the middle of the sample. ξ defined above controls the width of the domain wall. Here $\xi = 3$ and $L_x = 50$. Periodic boundary conditions on the x axis. Other model parameters are $\epsilon = 4$, $B = 0.001$ $L_y = 8$, $L_z = 100$.

The change in θ due to m_5 is $\Delta\theta = \frac{4\pi^2}{BL_z}Q$, Q is the sum of the charge density from $x = 0$ to $x = \frac{L_x}{2}$ for some y. We get

$$\begin{aligned} \Delta\theta_{\xi=1,L_x=40} &= 0.214 \\ \Delta\theta_{\xi=2,L_x=40} &= 0.220 \\ \Delta\theta_{\xi=3,L_x=50} &= 0.213. \end{aligned} \tag{5.5}$$

(for $\xi = 3$ we use $L_x = 50$, as with $L_x = 40$ the charge distributions from the two domain walls starts to overlap). In the original setup (m_5 zero on half the sample) we had

$$\Delta\theta_{m_5,0} = 0.215. \tag{5.6}$$

Next we look at the flux insertion setup depicted in Fig. 3.2, with a constant $m_5 = 0.1$ in the bulk, open boundary conditions, $L = 16$, $\Omega = 1$ (additional

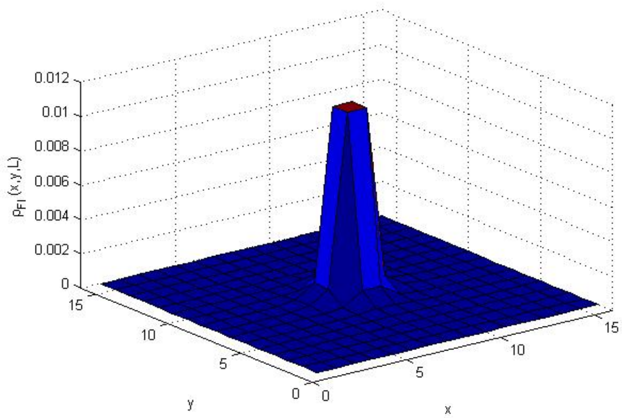

Figure 5.9: Charge density for the flux insertion setup. The top surface of the sample is shown. $m_5 = 0.1$ in the entire sample. $L = 16$. $\Phi = \eta\Phi_0$ is the magnetic flux inside the tube, $\eta = 0.1$. $\Omega = 1$ is the magnitude of the time reversal breaking on the surface. To get to charge accumulated on the flux tube we sum the charge on the entire upper half of the sample.

time reversal breaking on the surface is needed here, as we use small m_5), and all other model parameters the same. The charge density on the top surface is shown in Fig. 5.9.

We calculate the charge Q_{FI} in the entire upper half of the sample ($z > \frac{L}{2}$). The lower half of the sample will have an opposite charge. To get the change in θ from the case with $m_5 = 0$ we use

$$\Delta\theta_{FI} = \frac{2\pi Q_{FI}}{\eta} - \pi. \tag{5.7}$$

$\Phi = \eta\Phi_0$ is the flux inside the flux tube. We get

$$\Delta\theta_{FI} = 0.223. \tag{5.8}$$

For the magnetic monopole setup we use $m_5 = 0.1$, open boundary conditions, $L = 16$ and all other model parameters the same. The magnetic monopole is located at the middle of the sample. Fig. 5.10 shows the charge

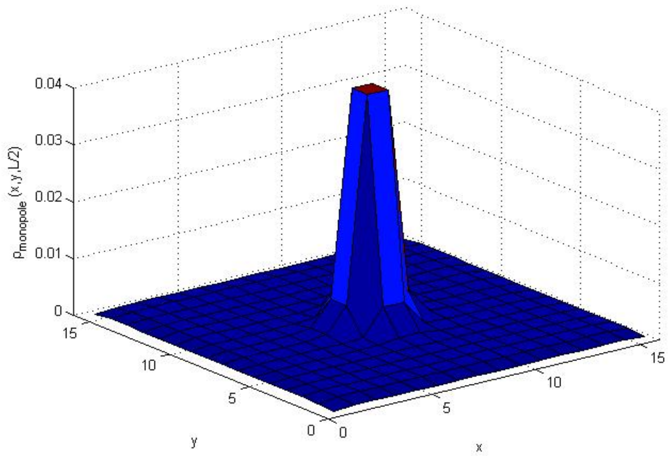

Figure 5.10: Charge density in the magnetic monopole setup. The $z = \frac{L}{2}$ surface is shown. $m_5 = 0.1$ in the entire sample. $L = 16$. The magnetic monopole is of unit magnetic charge.

density for the $z = \frac{L}{2}$ plane. The charge accumulated up to distance R from the monopole is shown in Fig. 5.11.

We take the charge accumulated on the magnetic monopole to be one of the points on the plateau from Fig. 5.11. We note that the charge on the entire sample is zero, here the negative counter part to the charge near the monopole is accumulated on the surface. Similarly to the flux insertion setup, to get the change in θ from the case with $m_5 = 0$ we use

$$\Delta\theta_{\text{monopole}} = 2\pi Q_{\text{monopole}} - \pi, \tag{5.9}$$

to get

$$\Delta\theta_{\text{monopole}} = 0.219. \tag{5.10}$$

The full Brillouin zone prediction with the same model parameters gives

$$\Delta\theta_{\text{Full BZ}} = 0.217. \tag{5.11}$$

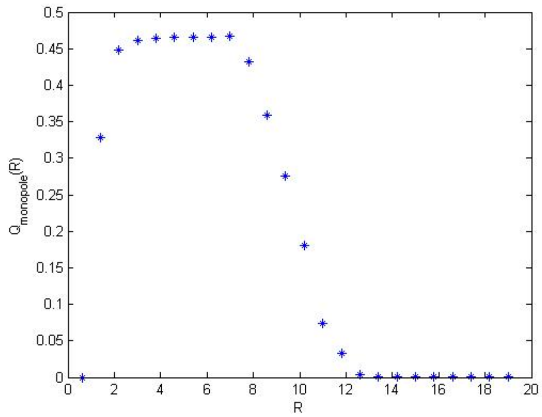

Figure 5.11: Charge accumulated up to distance R from a unit magnetic monopole Vs. R. $m_5 = 0.1$, $\epsilon = 4$, $L = 16$. We take the charge accumulated on the monopole from the plateau of $R \simeq 4$ to $R \simeq 6$. For large R the charge goes to 0 as the total charge in the sample is zero (that is, the same as in the case with $m_5 = 0$ or without the magnetic monopole).

The low energy prediction is

$$\begin{aligned}\Delta\theta_{\text{Low E}} = &\arctan\left(\frac{0.1}{10}\right) - 3\arctan\left(\frac{0.1}{6}\right) \\ &+3\arctan\left(\frac{0.1}{2}\right) - \arctan\left(\frac{0.1}{-2}\right) = 0.159.\end{aligned} \tag{5.12}$$

We sum the results in the following table

	numerical calculations	Full BZ prediction	Low E prediction
$\Delta\theta$	0.213 - 0.223	0.217	0.159

We see that all the different numerical calculations agree with each other, and with the full Brillouin zone prediction, and that there is a deviation from the low energy prediction. We get similar behavior for different model parameters. We also tried using different boundary conditions where possible, as explained in the model description section, the results does not change significantly. This supports the conclusion that the low energy prediction is an approximation.

Chapter 6

Conclusions

The main goal of this work was to numerically calculate θ in a system with broken $\mathcal{P}$ and $\mathcal{T}$, and compare the result with the theoretical prediction coming from various field theory and band structure calculations. Different low energy calculations yield the simple result, saying that the contribution to θ from each Γ point is the phase of the complex mass, $m = m_0 + im_5$, at the Γ point (up to a constant being either 0 of π).

The numerical results show a good but not exact agreement with the prediction coming from low energy calculations, and an exact agreement with a calculation taking into account the full Brillouin zone.

We do not have an analytical form for the exact form θ takes. For Dirac Hamiltonian models this exact form can be evaluated numerically relatively easily using the integral

$$\theta = \frac{1}{4\pi}\int_{BZ} d^3k \frac{2|d| + d_4}{\left(|d| + d_4\right)^2 |d|^3} \epsilon^{ijkl} d_i \partial_{k_x} d_j \partial_{k_y} d_k \partial_{k_z} d_l.$$

with the simple low energy result usually being an approximation. The special role d_4 takes here is assuming that in the Dirac Hamiltonian, Γ_4 is invariant under time reversal and parity.

As mentioned, for a number of topological insulator models describing real materials, m_5 is related to anti-ferromagnetic order. In those cases we conclude that anti-ferromagnetic order will change the magnitude of the magneto-electric effects. This change could be calculated or approximated using the methods described above.

Bibliography

[1] Xiao-Liang Qi, Taylor L. Hughes, and Shou-Cheng Zhang. Topological field theory of time-reversal invariant insulators. *PRB*, 78(195424), 2008. → pages 1, 5, 6, 14, 31, 32

[2] A. M. Essin, J. E. Moore, and D. Vanderbilt. Magnetoelectric polarizability and axion electrodynamics in crystalline insulators. *PRL*, 102(146805), 2009. → pages 1

[3] R. D. Peccei and H. R. Quinn. Cp conservation in the presence of pseudoparticles. *PRL*, 38(1440), 1977. → pages 2

[4] S. Weinber. A new light boson? *PRL*, 40(223), 1978. → pages 2

[5] F.Wilczek. Problem of strong p and t invariance in the presence of instantons. *PRL*, 40(279), 1978. → pages 2

[6] F. Wilczek. Two applications of axion electrodynamics. *PRL*, 58(18), 1987. → pages 2

[7] L. D. Duffy and K. van Bibber. Axions as dark matter particles. *New journal of physics*, 11(105008), 2009. → pages 2

[8] L. D. Duffy, P. Sikivie, D. B. Tanner, S. J. Asztalos, C. Hagmann, D. Kinion, L. J. Rosenberg, K. van Bibber, D. B. Yu, , and R. F. Bradley. High resolution search for dark-matter axions. *PRD*, 74(012006), 2006. → pages 2

[9] W. Beiglbck R. Beig and W. Domcke. *Axions: Theory, Cosmology, and Experimental Searches*. Springer, New York, 2008. → pages 2

[10] M.M. Vazifeh and M. Franz. Quantization and 2pi periodicity of the axion action in topological insulators. *PRB*, 82(233103), 2010. → pages 2

[11] L. Fu, C. L. Kane, and E. J. Mele. Topological insulators in three dimensions. *PRL*, 98(106803), 2007. → pages 3, 4

[12] L. Fu and C. L. Kane. Topological insulators with inversion symmetry. *PRB*, 76(045302), 2007. → pages 3, 4, 16, 26

[13] D. Hsieh, D. Qian, Y. Xia L. Wray, Y. S. Hor, R. J. Cava, and M. Z. Hasan. A topological dirac insulator in a quantum spin hall phase. *Nature (London)*, 452(970), 2008. → pages 3

[14] Y. Xia, D. Qian, D. Hsieh, L. Wray, A. Pal, H. Lin, A. Bansil, D. Grauer, Y. S. Hor, R. J. Cava, and M. Z. Hasan. Observation of a large-gap topological-insulator class with a single dirac cone on the surface. *Nature Physics*, 5(398), 2009. → pages 3

[15] Y. L. Chen, J. G. Analytis, J.-H. Chu, Z. K. Liu, S.-K. Mo, X. L. Qi, H. J. Zhang, D. H. Lu, X. Dai, Z. Fang, S. C. Zhang, I. R. Fisher, Z. Hussain, and Z.-X. Shen. Experimental realization of a three-dimensional topological insulator, bi2te3. *Science*, 325(178), 2009. → pages 3

[16] L. Fu and C. L. Kane. Time reversal polarization and a z2 adiabatic spin pump. *PRB*, 74(195312), 2006. → pages 4

[17] Zhong Wang, Xiao-Liang Qi, and Shou-Cheng Zhang. Equivalent topological invariants of topological insulators. *New journal of physics*, 12(065007), 2010. → pages 4

[18] Rundong Li, Jing Wang, Xiao-Liang Qi, and Shou-Cheng Zhang. Dynamical axion field in topological magnetic insulators. *Nature Physics*, (1534), 2010. → pages 4, 5, 30, 31, 33

[19] Michael Mulligan and F. J. Burnell. Topological insulators avoid the parity anomaly. *PRB*, 88(085104), 2013. → pages 4, 11

[20] J. Goldstone and F. Wilczek. Fractional quantum numbers on solitons. *PRL*, 47(14), 1981. → pages 5, 8

[21] G. Rosenberg and M. Franz. Witten effect in a crystalline topological insulator. *PRB*, 82(035105), 2010. → pages 5, 12, 15, 27

[22] E. Wittten. *PRL*, 86(283), 1979. → pages 5, 27

[23] G. Rosenberg, H.-M. Guo, and M. Franz. Wormhole effect in a strong topological insulator. *PRB*, 82(041104(R)), 2010. → pages 5, 12, 24, 25, 26, 27

[24] K. Fujikawa and H. Suzuki. *Path Integrals and Quantum Anomalies.* Oxford University Press, 2004. → pages 7

[25] M. E. Peskin and D. V. Schroeder. *An Introduction to Quantum Field Theory.* Perseus Press, Cambridge, MA, 1995. → pages 33